

# Development of a beam-based phase feed-forward demonstration at the CLIC Test Facility (CTF3).

Jack Roberts  
New College, Oxford

Thesis submitted in fulfilment of the requirements for the degree of Doctor of Philosophy at the University of Oxford

Trinity Term, 2016

## **Abstract**

This is the abstract TeX for the thesis and the stand-alone abstract.

# Acknowledgements

Acknowledgements.

# Contents

<b>1</b>	<b>Phase Monitor Performance</b>	<b>1</b>
1.1	Phase Monitor Design . . . . .	1
1.2	Phase Monitor Electronics . . . . .	7
1.3	Resolution Definition . . . . .	12
1.4	Digitisation of Phase Monitor Signals . . . . .	15
1.5	Fitting Method . . . . .	17
1.6	Signal Generator Measurements . . . . .	19
1.6.1	Experimental Setup . . . . .	19
1.6.2	Results . . . . .	20
1.6.3	Mixer Performance . . . . .	20
1.6.4	Diode Performance . . . . .	28
1.6.5	Consequences for Normal Operation . . . . .	34
1.7	Calibrations . . . . .	35
1.7.1	Calibration on SiS Digitisers . . . . .	36
1.7.2	Calibration on FONT5a Board . . . . .	39
1.7.3	Multi-Sample Results . . . . .	39
1.7.4	Zero Crossing . . . . .	41
1.8	Phase Shifter Noise . . . . .	43
1.9	Resolution Measurements . . . . .	49
1.9.1	Best Resolution . . . . .	49
1.9.2	With Sample Averaging . . . . .	50
1.9.3	Dependence of Resolution on LO Phase . . . . .	50
1.10	Bandwidth . . . . .	51
1.11	Comparison of Measured Phase Along Pulse . . . . .	51
1.12	Effect of Variations in Calibration Constant . . . . .	56
1.13	Dependence on Position . . . . .	56
	<b>Bibliography</b>	<b>63</b>

# Chapter 1

## Phase Monitor Performance

In order to successfully correct the phase with the PFF system it is clearly necessary to be able to accurately measure the phase, whilst meeting the low latency (380 ns for the complete system) and high bandwidth (30 MHz) requirements of the correction. Purpose-built phase monitors for the PFF system have been designed and constructed by INFN, Italy [REF]. Three of these monitors are currently installed at CTF3 — two in the CT line at the end of the linac and one after the TL2 chicane in the TBL line. The approximate positions of the monitors are shown on the CTF3 layout in Figure [REF]. The two “upstream” phase monitors in the CT line will be referred to as Mon 1 and Mon 2 (Mon 1 being before Mon 2 in the beam line) in this chapter. The “downstream” phase monitor in TBL will be referred to as Mon 3. Mon 1 is normally used as the PFF correction input, with the neighbouring Mon 2 used for performance cross-checks. Mon 3 is then used to measure the effect of the PFF correction. In the rest of the thesis the phase measurements are generally simply referred to as being from either one of the upstream phase monitors, or the downstream monitor.

The chapter begins with an overview of the design and installation of the phase monitors themselves as well as the associated electronics. The remainder of the chapter then focuses on operational procedures, measurements of the performance of the phase monitors and the changes that have been made in order to improve it. The headline result for the chapter is the achieved resolution of below 0.14° in Section 1.9, which is derived to be necessary to be able to achieve the targeted 0.2° corrected phase jitter in Section 1.3. Several effects have also been identified that can still degrade the accuracy of the phase measurement, such as the position dependence seen in Section 1.13. These are the first areas that should be looked at if an improvement in phase monitor performance is necessary for future PFF tests.

### 1.1 Phase Monitor Design

The phase monitors are cylindrical cavities with a length of approximately 19 cm and an internal diameter of 23 mm, as shown in Figure 1.1. When a charged beam traverses a cavity the interaction of the beam with the cavity walls creates electromagnetic fields inside the

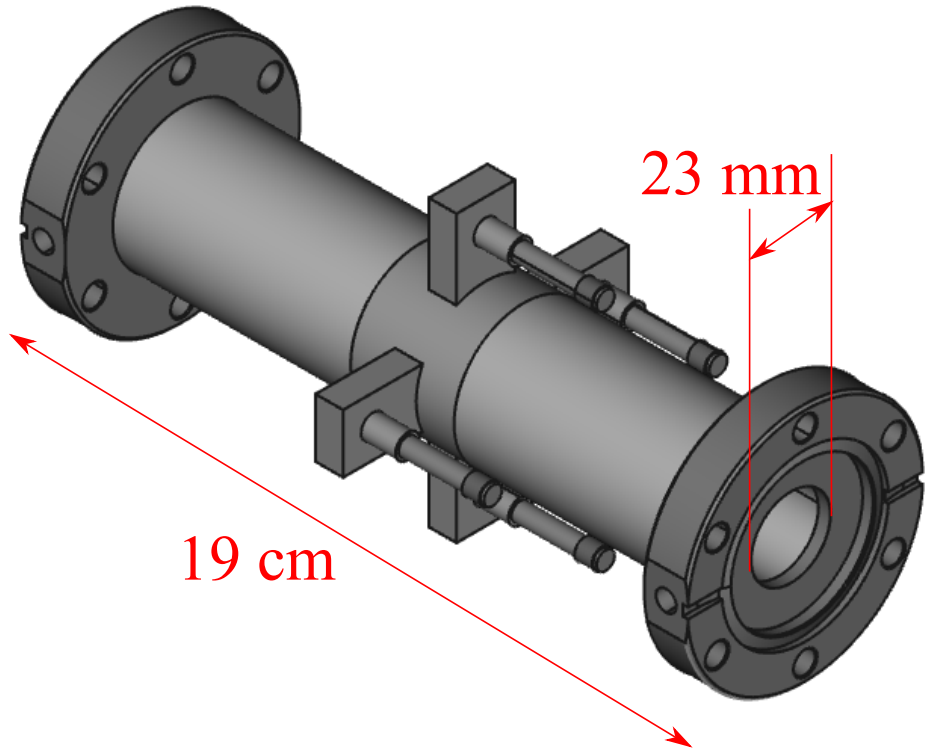


Figure 1.1: Technical drawing of the phase monitor cavity design [REF]. The length and internal diameter of the monitor is shown. Around the centre of the monitor are the four evenly spaced RF feedthroughs.

cavity. The amplitude of the induced fields depends both on the bunch charge and the bunch length [REF]. Small ridges (called notch filters) in the cavity create a volume resonating at 12 GHz (the CLIC combined bunch frequency) that contains the beam induced fields and reflects any stray 12 GHz fields not associated with the beam outside the cavity. This is shown in Figure 1.2. Four rectangular slots, arranged in horizontal and vertical pairs, around the mid-point of the cavity are then used to extract the beam induced resonant fields. The fields leaving the cavity are transported in short rectangular waveguides before a transition to a  $50 \Omega$  coaxial cable via an RF feedthrough [REF]. The output of the phase monitor cavities is therefore four 12 GHz signals whose time structure depends on the arrival time, or phase, of the drive beam bunches.

The solutions to Maxwell's equations in cavities such as this give a discrete set of transverse electric (TE) and transverse magnetic (TM) modes dependent on the geometry of the cavity [REF]. TE modes are characterised by having only transverse electric field components, and no longitudinal electric field component, whereas TM modes have only transverse magnetic field components and no longitudinal magnetic field component. Each TM and TE mode has an associated cutoff frequency dependent on the number of half-period variations,  $n$  and  $m$ , in the field horizontally and vertically across the cavity respectively. The amplitude of the 12 GHz signals output from the cavity will contain components of each TM and TE mode with a cutoff frequency below 12 GHz. For cylindrical cavities the cutoff frequency of

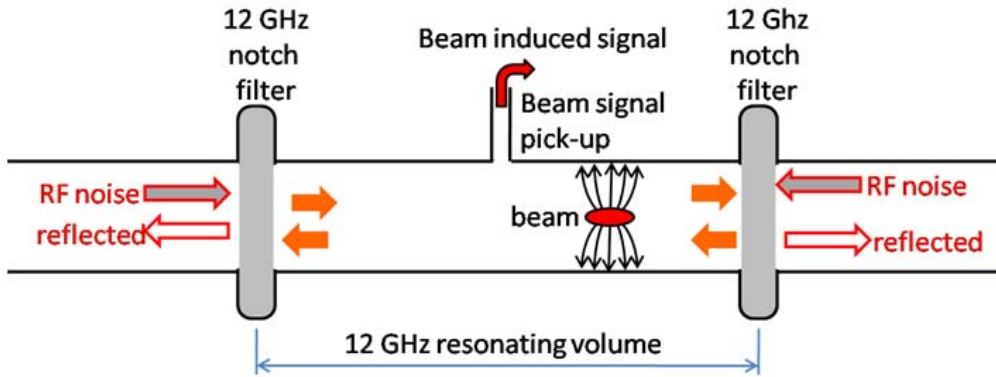


Figure 1.2: Schematic of phase monitor design [REF].

the TM is defined as [REF]:

$$f_{nm} = \frac{c}{2\pi} \frac{p_{nm}}{a} \quad (1.1)$$

And for the TE modes as:

$$f_{nm} = \frac{c}{2\pi} \frac{p'_{nm}}{a} \quad (1.2)$$

Where  $a$  is the radius of the cavity,  $p_{nm}$  is the  $m^{\text{th}}$  zero of the Bessel function  $J_n(x)$ , and  $p'_{nm}$  is the  $m^{\text{th}}$  zero of the derivative of the Bessel function  $J'_n(x)$  [REF]. The beam pipe around the location of the phase monitors at CTF3 is usually 4 cm in diameter, and a cavity of this size would support six separate TM or TE modes with a cutoff frequency below 12 GHz [REF]. It is for this reason that the phase monitor diameter was reduced to 23 mm, where only two modes are present: TM01 ( $n = 0$ ,  $m = 1$ ,  $p_{01} = 2.4$ ) and TE11 ( $n = 1$ ,  $m = 1$ ,  $p'_{11} = 1.8$ ).

TM01 is referred to as the monopole mode and TE11 as the dipole mode. The induced field distribution resulting from a bunch entering the cavity for both modes is shown in Figure 1.3. The precise expressions for each field distribution can be found in [REF]. When the beam has been correctly setup it should enter the phase monitor cavity close to its centre. For small (horizontal or vertical) offsets between the beam position and the cavity centre there is no dependence of the monopole mode amplitude on the incoming beam position. However, the amplitude of the dipole mode does depend on the beam position, even for small offsets from the cavity centre. This means the amplitude of any of the four individual RF outputs from the monitor will have a position dependence. This property is used in cavity beam position monitors (BPMs) [REF], but is undesirable for a phase monitor where the measurement should be position independent. For a 1 mm beam position offset the dipole mode is expected to have around 10% the amplitude of the monopole mode [REF].

To remove the unwanted dipole mode the horizontal and vertical pairs of outputs from the cavities can be combined, as the mode is symmetric and has equal magnitude but opposite sign on each side of the cavity. As the CTF3 beam is generally more stable in the vertical plane (as the majority of bends in the beam line are horizontal the energy related orbit jitter resulting from dispersion is larger in the horizontal plane) the vertical pair of RF feedthroughs from the monitors are normally used. The two outputs are summed using 180 degree hybrids [REF] installed next to the phase monitor cavities in the machine hall.

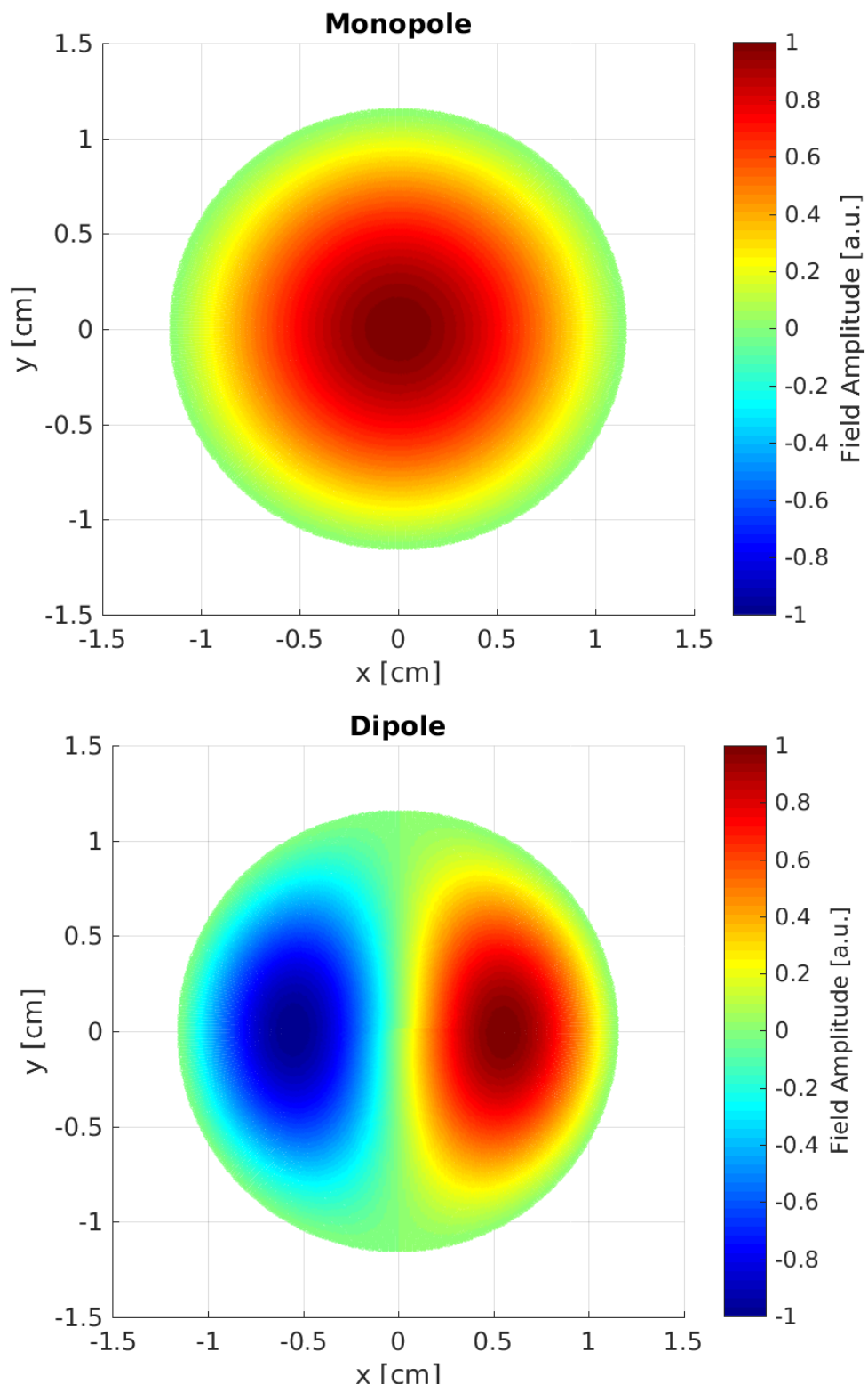


Figure 1.3: Field distribution of Monopole (TM01) and dipole (TE11) modes in the phase monitor cavities. The dipole mode has both horizontal and vertical components - only the horizontal component is shown.

Monitor	Power
Mon 1	27.6 dBm
Mon 2	29.8 dBm
Mon 3	24.5 dBm

Table 1.1: Power of the phase monitor signals (hybrid sum outputs) measured in the klystron gallery prior to being processed by the phase monitor electronics.

The horizontal pair is also instrumented in the same way but the outputs are typically not used. For an ideal (perfectly symmetric) cavity and hybrid this would create an output with only the position independent monopole mode present. In reality small misalignments, for example in the waveguides and RF feedthroughs, cause slight asymmetries in the cavity and signal combination which leaves a small residual dipole component. The signal combination in the hybrids is expected to reduce the dipole amplitude by a further 20 dB at a 1 mm offset, giving a final amplitude around 1% of the monopole mode [REF]. The remaining position dependence of the phase measurement is discussed in Section 1.13. How the output from the hybrids is processed to calculate the phase is discussed in the next section.

Figure 1.4 shows the installation of the upstream phase monitors in the CT line. The installation allows up to three phase monitors to be installed neighbouring each other, with the current two monitors installed in the first and third slots leaving approximately a 20 cm gap between the two. The connections between the four RF feedthroughs on the monitors and the hybrids fixed underneath the monitors can be seen in the figure, with the hybrids combining the horizontal pairs visible and two further hybrids placed on the other side of the beam line for the vertical pairs. The outputs from the hybrids are routed up to the klystron gallery on the floor above the accelerator hall, where they are processed and used for the PFF inputs. The overall phase monitor setup including the cables adds around 50 ns to the overall PFF latency [REF]. For reference the power level of the three phase monitor signals as measured once they reach the klystron gallery are quoted in Table 1.1. These are useful to interpret the results of Section 1.6, for example.

## 1.1 Phase Monitor Design

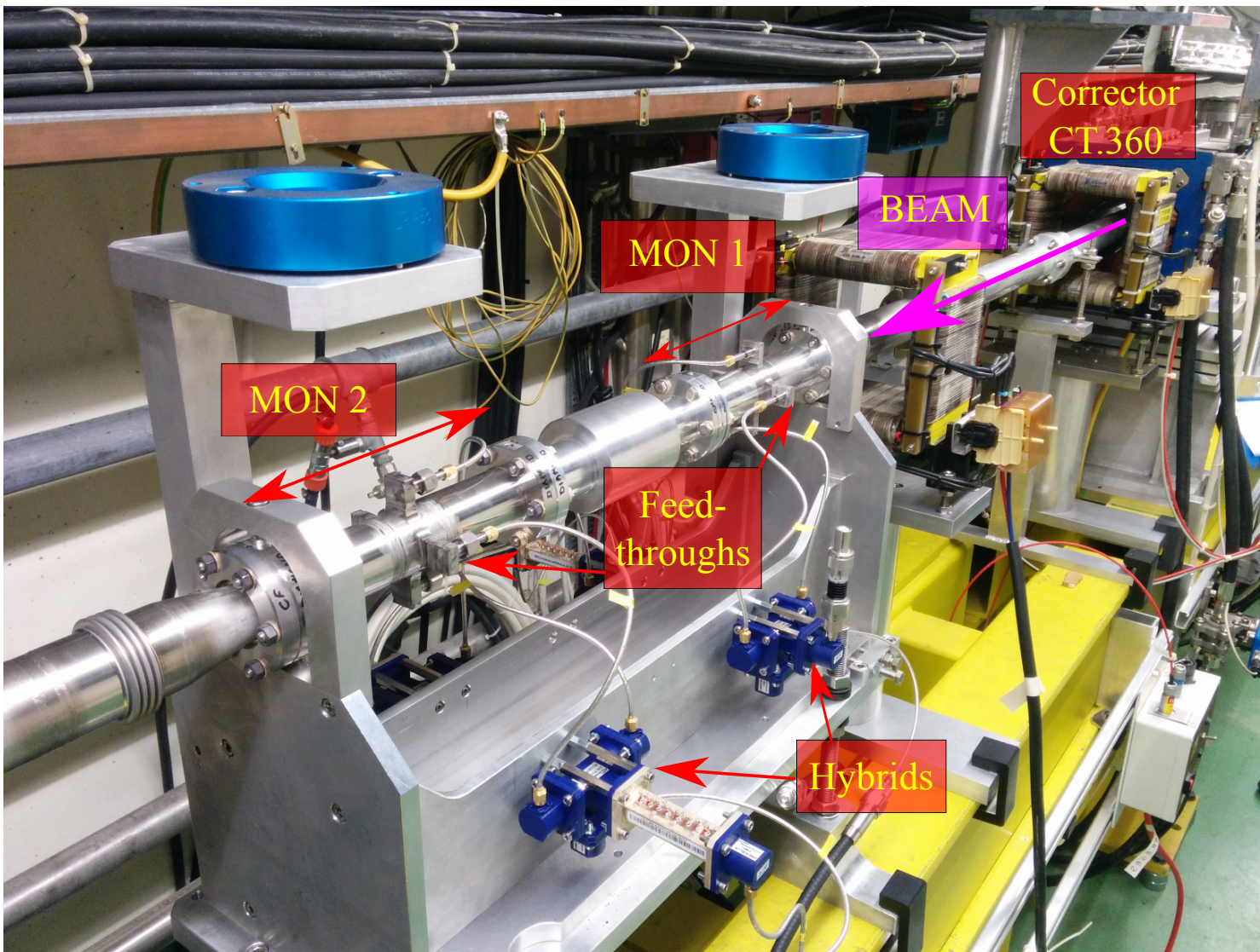


Figure 1.4: Annotated picture of the two upstream phase monitors installed in the machine.

## 1.2 Phase Monitor Electronics

The output of the phase monitor cavities (or more precisely the combined output from the hybrids) is a sinusoidal signal with a frequency of  $\omega_{RF} = 11.994$  GHz (the precise CLIC combined drive beam bunch frequency is 11.994 GHz rather than 12 GHz). This can be expressed as follows:

$$RF(t) = A_{RF}(t) \cos[\omega_{RF}t + \phi(t)] \quad (1.3)$$

Where  $A_{RF}(t)$  is the time dependent amplitude (voltage) of the phase monitor signal and  $\phi(t)$  is the time dependent beam phase of interest for the PFF system. The beam based signals from the phase monitors are referred to as the RF signals.

This high frequency signal cannot be digitised directly so in order to extract the phase dependence it is combined with a similar reference signal to create a low, or intermediate, frequency signal that can be digitised and preserves the beam phase information. The devices that “mix” the beam signal with the reference signal are called mixers. The reference signal is referred to as the local oscillator or LO signal. The LO is usually a continuous sinusoidal signal with constant amplitude  $A_{LO}$  and frequency  $\omega_{LO}$ :

$$LO(t) = A_{LO} \cos[\omega_{LO}t] \quad (1.4)$$

The mixer multiplies the RF and LO signals, to create an output with the following dependence on each signal:

$$\text{Mixer}(t) = RF(t) \times LO(t) \quad (1.5)$$

$$\text{Mixer}(t) = A_{RF}(t)A_{LO} \cos[\omega_{RF}t + \phi(t)] \cos[\omega_{LO}t] \quad (1.6)$$

Using trigonometric identities this can be expressed in terms of a high frequency component, with a frequency of  $(\omega_{LO} + \omega_{RF})$ , and a low frequency component, with a frequency of  $(\omega_{LO} - \omega_{RF})$ :

$$\text{Mixer}(t) = \frac{A_{RF}(t)A_{LO}}{2} \{\cos[(\omega_{LO} + \omega_{RF})t + \phi(t)] + \cos[(\omega_{LO} - \omega_{RF})t + \phi(t)]\} \quad (1.7)$$

The high frequency component can then easily be removed using a low pass filter, so that the mixer output becomes:

$$\text{Mixer}(t) = \frac{A_{RF}(t)A_{LO}}{2} \cos[(\omega_{LO} - \omega_{RF})t + \phi(t)] \quad (1.8)$$

Finally, by using a reference LO signal which has the same frequency as the RF signal, which is the case for the phase monitor electronics presented here, this simplifies to:

$$\text{Mixer}(t) = \frac{A_{RF}(t)A_{LO}}{2} \cos[\phi(t)] \quad (1.9)$$

The resulting mixer output is therefore a low frequency signal that depends only on the amplitude of the RF signal and the phase (as well as the constant LO amplitude).

To use the mixer output to calculate the phase the voltage of the RF signal,  $A_{RF}$ , must be known. This can be determined by splitting the RF signal between the mixer and a diode detector, whose output is dependent on the power of the signal (the square of the voltage):

$$\text{Diode}(t) = A_{RF}(t)^2 \quad (1.10)$$

The phase can then be reconstructed from the mixer and diode outputs as follows:

$$\frac{\text{Mixer}(t)}{\sqrt{\text{Diode}(t)}} = A \cos[\phi(t)] \quad (1.11)$$

$$\phi(t) = \arccos \left[ \frac{\text{Mixer}(t)}{A \sqrt{\text{Diode}(t)}} \right] \quad (1.12)$$

Where  $A$  is a calibration constant dependent on the relative amplitudes of the mixer and diode outputs. The electronics for the three PFF phase monitors use mixers and diodes as described above to produce signals that are dependent on the phase and amplitude of the output from the phase monitor cavities. Figure 1.5 shows the front panel of one of the sets of the electronics, showing the RF and LO inputs and mixer and diode outputs. The mixer and diode outputs are digitised, with the phase calculation above performed after the digitisation rather than by the phase monitor electronics themselves.

In order to achieve resolutions below  $0.2^\circ$ , as necessary for the PFF system (Section 1.3), the electronics do not work exactly as described above but instead use multiple mixers and diodes. Non-linearities in the response of mixers and diodes are typically worse at higher input powers [REF], but higher input powers are desirable to improve the signal to noise ratio of the output. With a single mixer and diode a compromise must therefore be made between the accuracy (linearity) and resolution (noise) of the device. To be able to operate the mixers at low power whilst maintaining a good signal to noise ratio eight separate mixers and diodes are used in each set of electronics [REF]. The RF and LO inputs are split between the eight mixers and diodes, and then the eight outputs of each type are added together to create the final mixer and diode outputs from the electronics. Figure 1.6 shows a simplified example of this with two mixers and diodes.

Figure 1.6 also shows all the elements present in the generation of the LO reference signal for the electronics. The LO signal for all three sets of electronics is generated from a common 3 GHz source that is locked to the timing of the CTF3 drive beam (which has a 3 GHz acceleration frequency). The 3 GHz signal is split in to three to provide the LO input for each set of electronics. After the split each LO chain includes a phase shifter, bandpass filter, frequency multiplier and an amplifier. The phase shifters are required for the calibration process as discussed in Section 1.7. Initially these were 3 GHz digital phase shifters of type [REF], but these were later replaced with passive mechanical phase shifters for the reasons seen in Section 1.8. The mechanical shifters are of type [REF], and can be changed in units of 0.02 degrees at 4 GHz. After the shifters, a bandpass filter [REF] removes any unwanted out of frequency noise in the LO signal, the frequency multiplier [REF] increases the frequency of the LO to 11.994 GHz and finally the amplifier [REF] is used to boost the power of the LO signals to the level seen in Table 1.2.



Figure 1.5: Front panel of the phase monitor electronics boxes containing the mixers and diodes. The connectors labelled LO and RF take the signals from the LO source and the phase monitors respectively. The connectors labelled  $A^2$  and  $A \sin(\phi)$  are the diode and mixer outputs respectively.

LO	Power
LO 1	22.6 dBm
LO 2	23.6 dBm
LO 3	25.5 dBm

Table 1.2: Power of the LO inputs to the phase monitor electronics.

Figure 1.7 finally shows the complete phase monitor electronics installation in the racks in the klystron gallery.

## 1.2 Phase Monitor Electronics

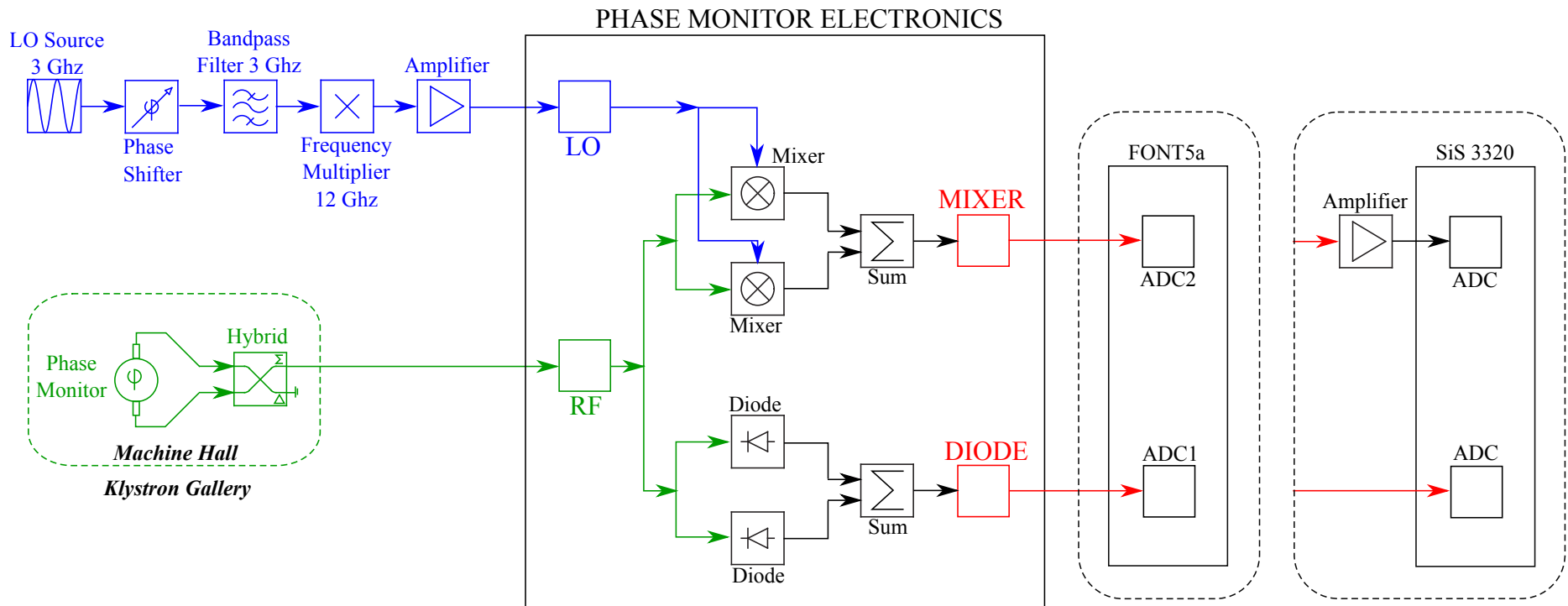


Figure 1.6: Simplified schematic of the phase monitor electronics setup. The components involved in the generation of the LO are shown in blue, the phase monitor beam signal in green and the outputs in red. For the purposes of the diagram only two individual mixers and diodes are shown. In the actual design the input signals are split between eight mixers and diodes, and then combined in the same way to create the two outputs. The outputs are digitised on either the FONT5a board or the SiS digitisers.

## 1.3 Resolution Definition

The performance of the PFF system clearly depends on the **accuracy** to which the phase can be measured. Many of the measurements in this chapter are therefore focused on the phase monitor resolution, or more precisely on the resolution of the combined phase monitor and electronics setup. The resolution is defined as the **jitter** between the measured phase and the true beam phase. This can be calculated by comparing the difference between the measured phase of two monitors. This is why two phase monitors, Mon 1 and Mon 2 are installed neighbouring each other in the upstream system in the CT line. The beam phase should be identical in these two monitors thus their measurements can always be compared to derive the resolution.

The precise derivation of the resolution dependent on the measurement of two monitors is as follows. First, the measured phase,  $\phi_x(t)$  and  $\phi_y(t)$ , in two monitors at time  $t$  can be defined as:

$$\phi_x(t) = \phi_b(t) + n_x(t) \quad (1.13)$$

$$\phi_y(t) = \phi_b(t) + n_y(t) \quad (1.14)$$

Where  $\phi_b(t)$  is the true beam phase and  $n_x(t)$  and  $n_y(t)$  is the noise on the measurement at that time. The time dependence will not be written explicitly from this point. These equations assume the beam phase is identical in each monitor, as should be the case for Mon 1 and Mon 2. The variance of each phase monitor measurement can then be derived from the equations above by adding the **variance of the beam phase and the noise in quadrature**:

$$\sigma_x^2 = \sigma_b^2 + \sigma_{nx}^2 \quad (1.15)$$

$$\sigma_y^2 = \sigma_b^2 + \sigma_{ny}^2 \quad (1.16)$$

Where  $\sigma_x$  and  $\sigma_y$  are the phase jitters measured by each phase monitor,  $\sigma_b$  is the true beam phase jitter and  $\sigma_{nx}$  and  $\sigma_{ny}$  are the phase monitor resolutions. Assuming each phase monitor has the same **resolution**,  $\sigma_n$ , this can be simplified to  $\sigma_x^2 = \sigma_y^2 = \sigma_b^2 + \sigma_n^2$ .

The quantity of interest for calculating the phase monitor resolution is the jitter in the difference between the two measured phases,  $\sigma_{x-y}$ . The variance of the difference between two correlated variables is defined as:

$$\sigma_{x-y}^2 = \sigma_x^2 + \sigma_y^2 - 2\sigma_x\sigma_y\rho_{xy} \quad (1.17)$$

$$(1.18)$$

Where  $\rho_{xy}$  is the correlation between the phase measurement of  $x$  and  $y$ . Substituting in the previously derived expressions for  $\sigma_x$  and  $\sigma_y$  this becomes:

$$\sigma_{x-y}^2 = 2(\sigma_b^2 + \sigma_n^2)(1 - \rho_{xy}) \quad (1.19)$$

The correlation coefficient  $\rho_{xy}$  depends on the covariance between  $x$  and  $y$ ,  $\text{cov}[x, y]$ , as follows:

$$\rho_{xy} = \frac{\text{cov}[x, y]}{\sigma_x\sigma_y} = \frac{\text{cov}[x, y]}{\sigma_b^2 + \sigma_n^2} \quad (1.20)$$

$$(1.21)$$

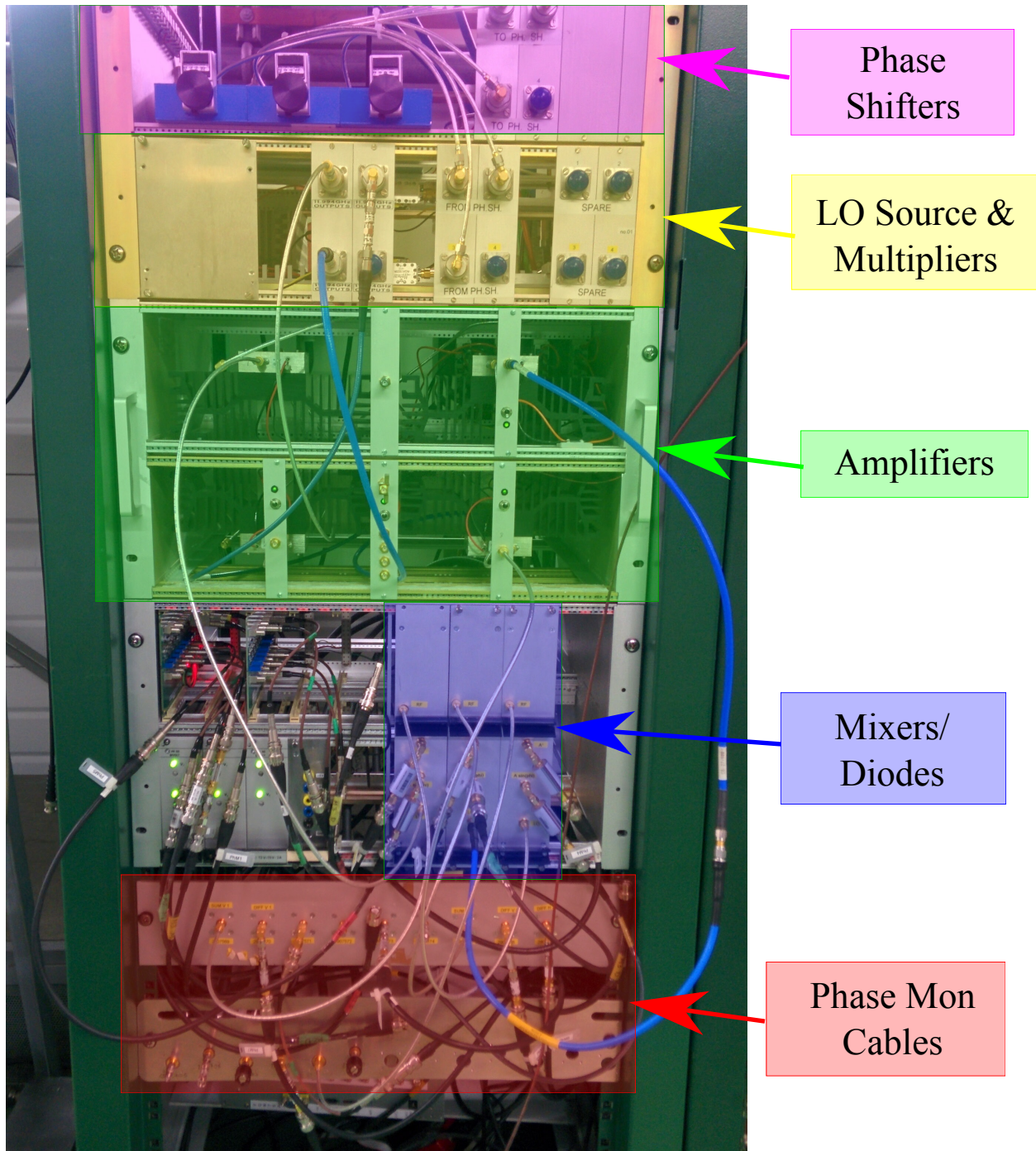


Figure 1.7: Annotated picture of the phase monitor electronics rack in the klystron gallery..

Where the covariance is defined as:

$$\text{cov}[x, y] = \frac{1}{N} \sum_{i=1}^N \phi_{xi} \phi_{yi} \quad (1.22)$$

$$(1.23)$$

Substituting in the expressions for  $\phi_x$  and  $\phi_y$  above and separating the terms in the sum then gives the following expression for the covariance of  $x$  and  $y$ :

$$\begin{aligned} \text{cov}[x, y] &= \frac{1}{N} \sum_{i=1}^N (\phi_{bi} + n_{xi})(\phi_{bi} + n_{yi}) \\ \text{cov}[x, y] &= \frac{1}{N} \sum_{i=1}^N \phi_{bi}^2 + \frac{1}{N} \sum_{i=1}^N \phi_{bi} n_{xi} + \frac{1}{N} \sum_{i=1}^N \phi_{bi} n_{yi} + \frac{1}{N} \sum_{i=1}^N n_{xi} n_{yi} \end{aligned} \quad (1.24)$$

The first term is the definition of the variance of the beam phase,  $\sigma_b^2$ . The remaining terms are the covariance between the beam phase and the monitor noises, and the covariance between the two monitor noises. Assuming the noise is uncorrelated all these terms are zero. The remaining equation for the covariance between  $x$  and  $y$  is therefore simply:  $\text{cov}[x, y] = \sigma_b^2$ . Finally, the correlation between the phase measurement of  $x$  and  $y$  becomes:

$$\rho_{xy} = \frac{\sigma_b^2}{\sigma_b^2 + \sigma_n^2} \quad (1.25)$$

Substituting this expression for the correlation in to the derived equation for the variance between the two phase measurements gives the following simple dependence on the phase monitor resolution:

$$\begin{aligned} \sigma_{x-y}^2 &= 2(\sigma_b^2 + \sigma_n^2) \left( 1 - \frac{\sigma_b^2}{\sigma_b^2 + \sigma_n^2} \right) \\ \sigma_{x-y}^2 &= 2\sigma_n^2 \end{aligned} \quad (1.26)$$

Finally, the resolution is defined as:

$$\sigma_n = \frac{\sigma_{x-y}}{\sqrt{2}} \quad (1.27)$$

In terms of a resolution calculation these equations only apply to the two upstream phase monitors. All the resolution values quoted in this chapter use this equation and the difference between the measurement of Mon 1 and Mon 2.

However, as the act of the PFF system can also be thought of as subtracting two phases (removing the upstream phase from the downstream phase) the same equations can be directly applied to determine the limitations that the phase monitor resolution places on the PFF performance. Equation 1.26 shows that the lowest possible corrected downstream phase jitter is a factor  $\sqrt{2}$  times larger than the phase monitor resolution. In order to reduce the downstream phase jitter to the CLIC target of  $0.2^\circ$  the phase monitor resolution must therefore be better than  $0.14^\circ$ . Equation 1.25 shows that with this  $0.14^\circ$  resolution and a typical beam phase jitter of  $0.8^\circ$  (Section ??) the measured correlation between two phase monitor measurements would be 97%.

Digitiser	No. ADCs	Resolution	Input Range	Sampling Rate	Bandwidth
SiS 3320	8	12-bit	$\pm 2.5$ V	up to 250 MHz	100 MHz
FONT5a	9	14-bit (13-bit used)	$\pm 0.5$ V	up to 400 MHz	1.4 GHz

Table 1.3: Specifications of the ADCs on the FONT5a board and SiS digitisers.

## 1.4 Digitisation of Phase Monitor Signals

The mixer and diode outputs from the phase monitor electronics must be digitised on analogue to digital converters (ADCs) so the signals can be processed and used for the PFF correction and offline data analysis. Two different types of ADCs have been used to digitise the phase monitor signals — the Texas Instruments ADS5474 ADCs [REF] on the purpose-built FONT5a board used as the PFF controller and a commercially available SiS 3320 digitiser [REF]. The design and use of the FONT5a board is discussed in more detail in Section ???. Table 1.3 summarises the specifications of each type of ADC.

The SiS digitisers are used in addition to the FONT5a board as the PFF correction running on the FONT5a board is operated as a standalone system independent from other acquisition systems at CTF3. The PFF algorithm requires only the signals from one of the upstream phase monitors to be connected to the FONT5a board, with the convention being to use Mon 1. Mon 2 and Mon 3 are then normally connected to the SiS digitisers instead. The SiS digitisers are setup with the same trigger and sampling frequency (192 MHz) used for other signals at CTF3, and data from them can be acquired together with other devices using the standard systems in place at CTF3. This allows the Mon 2 and Mon 3 signals to be easily compared to other measurements, such as beam position signals, which has been indispensable for optimising the setup of the PFF system and in particular the phase propagation (Chater ??).

Digitising the phase monitor signals contributes additional noise to the overall phase monitor electronics setup. The purpose of this section is to ensure that the digitiser noise makes only a negligible contribution to the resolution on the phase measurement. The main parameters of interest needed to determine this are the input range and resolution of the ADCs, with the SiS ADCs being 12-bit with a range of  $\pm 2.5$  V and the FONT5a ADCs being 13-bit with an input range of  $\pm 0.5$  V. The full 5 V peak-to-peak input range of the SiS ADCs is therefore split across  $2^{12} = 4096$  values, or ADC ‘counts’, with each count corresponding to roughly 1.2 mV. The equivalent 1 V peak-to-peak range and  $2^{13} = 8192$  counts of the FONT5a board corresponds to a factor 10 lower interval of 0.12 mV per ADC count. The voltage jitter added by the digitisation of the phase monitor signals cannot be expected to be better than 1 count. This already indicates that the FONT5a board should give a much lower contribution to the phase resolution than the SiS digitisers.

Figure 1.8 shows the ADC noise, converted from counts in to an equivalent voltage, for both the SiS and FONT5a ADCs. As expected the noise on the FONT5a board is much lower than on the SiS digitisers. The actual ADC jitter values are  $1.47 \pm 0.04$  counts or  $0.179 \pm 0.005$  mV on the FONT5a board, and  $1.11 \pm 0.03$  counts or  $1.36 \pm 0.03$  mV on the

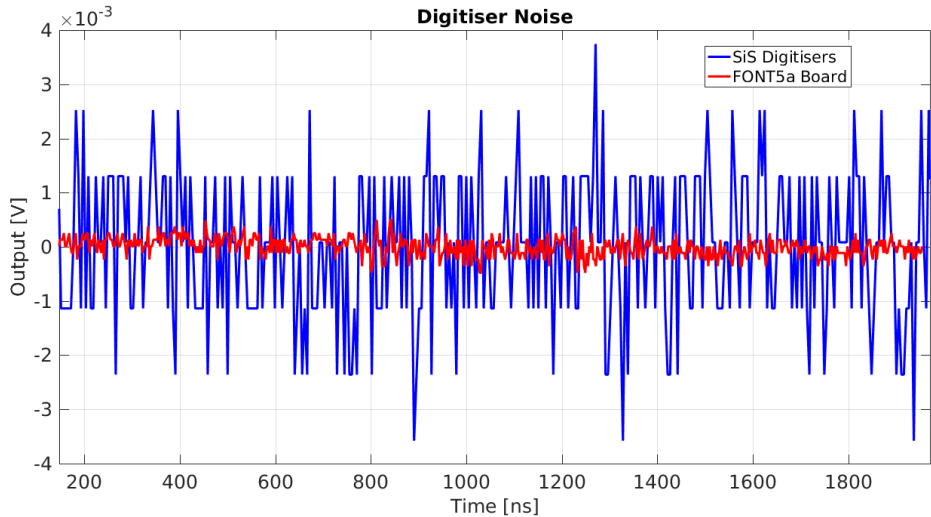


Figure 1.8: Comparison of noise on the output of the SiS and FONT5a ADCs.

SiS digitisers. These values can be converted in to an equivalent phase jitter using the phase reconstruction method described later in Section 1.6.5 and the monitor calibration constants determined in Section 1.7. For reference the peak output of the three phase monitor mixers varies between approximately 400 mV and 500 mV, which is well matched to the input range of the FONT5a ADCs. Taking the worst case scenario of Mon 3, which gives the lowest output voltage, the ADC jitter corresponds to  $0.0245 \pm 0.0007^\circ$  on the FONT5a board but  $0.198 \pm 0.005^\circ$  on the SiS digitisers. These values are summarised in Table 1.4.

As derived in the previous section the phase resolution must be better than  $0.14^\circ$  in order to achieve a corrected downstream phase jitter of  $0.2^\circ$  with the PFF system. The  $\sim 0.02^\circ$  contribution of ADC noise on the FONT5a board is therefore insignificant compared to the resolution requirements. However, although it does not directly impact the PFF performance the  $\sim 0.2^\circ$  ADC jitter on the SiS digitisers would greatly degrade the resolution of the measurements of Mon 2 and Mon 3 usually connected to the SiS digitisers and used for offline data analysis of the PFF results.

The high phase jitter contribution from the SiS digitisers originates from the roughly 500 mV maximum mixer output being much lower than the SiS ADC range of  $\pm 2.5$  V. In order to rectify this the mixer outputs are boosted by roughly a factor 2.5 in voltage using an amplifier prior to the SiS digitisers. The specifications of the amplifier used are documented in [REF]. With the amplifier in place the peak signal level sent to the SiS digitisers is around 1 V, and the equivalent phase jitter is reduced to  $0.078 \pm 0.002^\circ$ . This no longer prevents  $0.14^\circ$  resolution from being achieved on measurements using the SiS digitisers, as proven later in Section 1.9. A small further improvement in measured resolution could be achieved using a different amplifier and boosting the peak output voltage closer to 2 V.

Digitiser	Jitter [counts]	Jitter [mV]	Phase Jitter [degrees]
FONT5a	$1.47 \pm 0.04$	$0.179 \pm 0.005$	$0.0245 \pm 0.0007$
SiS 3320	$1.11 \pm 0.03$	$1.36 \pm 0.03$	$0.198 \pm 0.005$
SiS 3320 Amplified	$1.11 \pm 0.03$	$1.36 \pm 0.03$	$0.078 \pm 0.002$

Table 1.4: ADC jitter on the FONT5a board, SiS digitisers and with the mixer outputs amplified prior to the SiS digitisers expressed in terms of ADC counts, volts and equivalent phase jitter.

## 1.5 Fitting Method

Due to the dependence of the mixer output on  $\cos(\phi)$  as seen in Section 1.2, many of the measurements in this chapter require a sinusoidal fit of the form:

$$y = A \sin(bx + c) + d \quad (1.28)$$

The use of sine rather than cosine makes no difference to the fitted amplitude,  $A$ , and offset,  $d$  which are usually the only parameters of interest in this chapter. It is also convenient to consider a mixer output of zero to correspond to zero phase (rather than  $90^\circ$  as in Equation 1.11). All the fits of this type have been performed using a weighted nonlinear least squares fit implemented in MatLab fitting libraries [?]. Each data point is weighted by the inverse of its standard error squared.

Care must be taken to select suitable initial values for the four parameters in the fit in order to avoid local minima and ensure a reasonable fit. This is particularly important for a sinusoidal fit as there are many solutions with different frequencies and phase offsets that can match the data. The frequency,  $b$ , is the most critical parameter but for all the applications in this chapter this is already known, e.g. from the properties of the used phase shifters. Initial values for the three remaining parameters are estimated as follows:

$$A = \frac{\max(y) - \min(y)}{2} \quad (1.29)$$

$$d = \frac{\max(y) + \min(y)}{2} \quad (1.30)$$

$$c = \arcsin\left(\frac{y - d}{A}\right) - bx \quad (1.31)$$

The initial amplitude,  $A$ , and offset,  $d$ , of the sine curve are simply determined by comparing the minimum and maximum output. These initial estimates are therefore highly biased by any large outliers around the minimum and maximum output, but this is rarely the case for the application here and these simple estimators are sufficient. Rearranging Equation 1.28 gives the expression for  $c$  above. Due to its use of  $\arcsin$  the equation is only valid in the first and fourth quadrants, between  $-\pi/2$  and  $+\pi/2$  where the gradient of the sine curve is positive. The  $y$  value at each data point is compared to its neighbours to determine whether it is on the rising slope. The initial value of  $c$  is the mean value calculated across all the data points that meet this criteria.

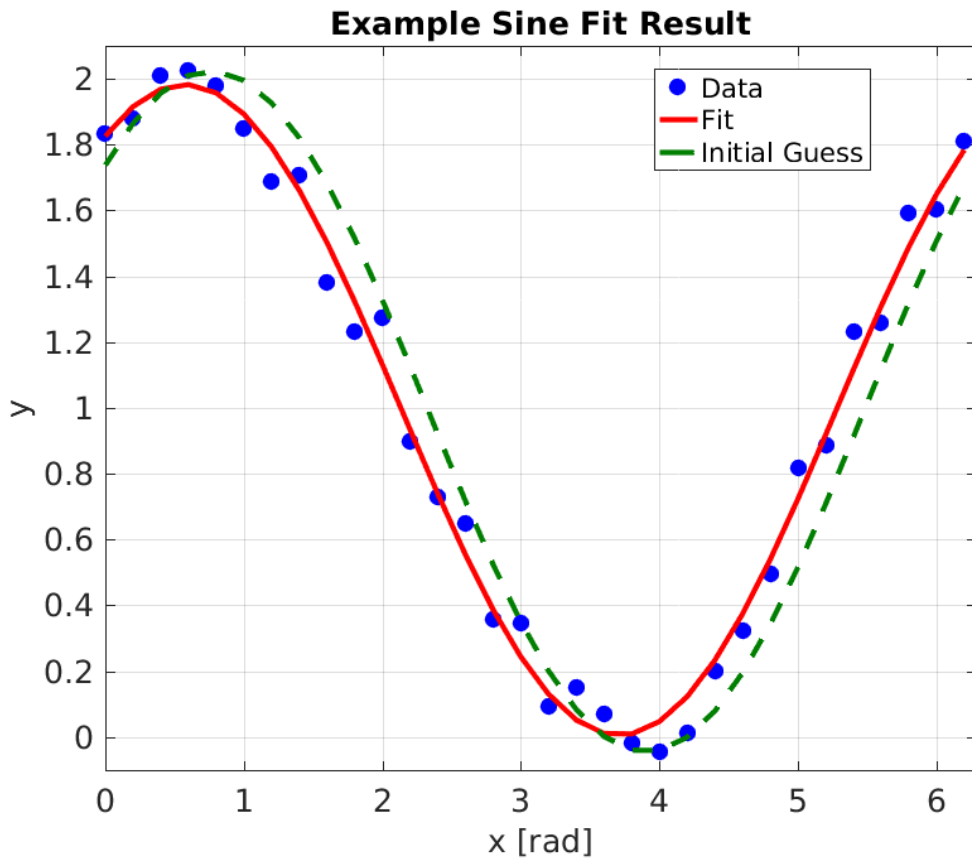


Figure 1.9: Example sine fit to generated data with added random noise.

Figure 1.9 and Table 1.5 show the results of an example fit using this approach. An initial distribution of points with  $y = \sin(x + 1) + 1$  is used ( $A = b = c = d = 1$ ), with random noise added.  $b$  is assumed to be known, as is normal. The initial estimates for  $A$  and  $d$  are within a few percent of their true value. The initial estimate for  $c$  is within 20% of the correct value. After fitting all four parameters are in agreement with the expected values within error bars.

Parameter	Value	Initial	Fit
$A$	1	1.03	$0.99 \pm 0.02$
$b$	1	1	$1.00 \pm 0.02$
$c$	1	0.81	$1.00 \pm 0.06$
$d$	1	0.99	$0.99 \pm 0.02$

Table 1.5: Typical upstream phase and energy conditions at CTF3.

## 1.6 Signal Generator Measurements

Measurements have been taken using a 12 GHz signal generator to determine the performance of the three sets of phase monitor electronics independently from the phase monitors themselves. In particular, these tests were focused on identifying the saturation and cross-talk characteristics of the output mixer and diode signals in order to determine a suitable input power range to use during normal operation.

### 1.6.1 Experimental Setup

Two changes were made to the setup shown in Figure 1.6 for these tests. Firstly, the beam induced signal from the phase monitors usually connected to the RF port of the mixers is replaced by the output from a 12 GHz signal generator. To be able to reach the same input power levels as the beam signals the signal generator output is amplified. This allowed the input power to the mixers to be varied in a wide range between 0 and 33dBm, or between 0.2 and 10.0 V in terms of voltage. The precise power sent to the mixer is verified between each measurement using a power meter.

Secondly, the diode outputs were amplified during these tests (using the same amplifier introduced in Section ??) by a factor 10 in voltage to reduce digitiser noise in the measurement. The non-amplified peak diode output is therefore 170 mV, rather than the 1.7 V seen in the plots in this section. The  $\pm 500$  mV mixer outputs have not been amplified. Usually the mixer output is amplified and the diode not amplified, as in Figure 1.6, for reasons that will become clear later in this chapter.

There are some differences between the properties of the generated signal and the beam signal that would be used in normal operation. Firstly, unlike the pulsed beam signal the used generated signal is continuous. It has been verified that the response of the mixers is equivalent for both the continuous and pulsed signals, at least in terms of output power and saturation levels [REF]. The cross-talk properties are difficult to characterise with beam based measurements alone, but assumed to be similar.

Secondly, the phase of the generated signal does not vary with time, compared to the beam signal which has a large  $\sim 40^\circ$  phase sag along the pulse and much larger phase jitter. If the signal generator was used at the same frequency as the beam and LO signals, 11.994 GHz, the mixer output would therefore be constant as it depends only on the static phase as per Equation 1.9. Instead, a generated signal with a slightly lower frequency of 11.991 GHz has been used. From Equation 1.8 it can be seen that in this case the mixer output voltage is sinusoidal, with a frequency equal to the frequency difference between the LO and RF inputs – or  $11.994 - 11.991$  GHz = 3 MHz with the setup used here. This has the benefit of being able to see the response of the electronics to all input phases in one measurement, rather than having to take multiple measurements varying the LO phase shifter between each one.

## 1.6.2 Results

Figures 1.10–1.15 show the mixer and diode outputs for all three sets of electronics at each of the input power levels sent from the signal generator. These will be referred back to and discussed in more detail in the remainder of this section. Some initial observations that are immediately clear from these figures are as follows. All mixer outputs show a sinusoidal oscillation with a frequency of 3 MHz, or 60 samples at the sampling frequency of 192 MHz, as expected. An oscillation with the same frequency is also visible on the diode outputs, with the largest amplitude for the 2nd set of electronics. This is the first hint of the non-ideal characteristics of the diodes. Finally, output of the mixer and diode increases with the input power, as expected. At high input powers the outputs begin to saturate. This is apparent by observing the diode signals, on which the output is much flatter at the highest power levels, without the oscillation seen at low input powers. The characteristics of the mixers are discussed in Section 1.6.3 and the diodes in Section 1.6.4.

## 1.6.3 Mixer Performance

### Sinusoidal Characteristics

Figure 1.16 shows fits to the response of all mixer outputs at an input power of 27 dBm, close to the typical input power from the beam signals when they are connected. Markers show the data points and the lines are sine fits to the data. The phase offset (displacement in peaks) between the output of each mixer holds no significance for the electronics performance. This is set only by the relative phase between the signal generator and the LO at the time the measurement was started. For normal operation with beam the LO phase shifters are changed to match the phasing of each set of electronics (Section 1.7).

The reconstruction of the phase from the mixer output depends on the mixer output being sinusoidal. In particular the maximum mixer output, or equivalently the gradient around zero mixer output (using the small angle approximation) is critical due to the dependence on the amplitude in Equation 1.12. Each set of electronics has a different output amplitude due to slight differences in the LO power for each set of electronics and between the individual components used. At an input power of 27 dBm Mixer 1 has a higher peak output of 510 mV, compared to 410 mV and 380 mV for Mixer 2 and Mixer 3 respectively.

Overall, the agreement between the actual mixer output and the sinusoidal fits at this input power is good. However, there is some distortion away from the ideal sine curve that is most visible around the maximum and minimum mixer output. Figure 1.17 shows the residuals between the mixer outputs and the sine fits across one half wavelength – from maximum output to minimum output. In the figure the plotted residual is the difference between the fit and the data expressed in terms of an equivalent phase offset,  $\Delta\phi$ , using:

$$\Delta\phi(t) = \arcsin\left(\frac{V_{MIXER}(t) - V_{FIT}(t)}{A}\right) \quad (1.32)$$

Where  $V_{MIXER}(t)$  and  $V_{FIT}(t)$  are the mixer voltage and fitted voltage at sample  $t$  respectively, and  $A$  is the fitted mixer amplitude. On the falling slope between the peaks there is

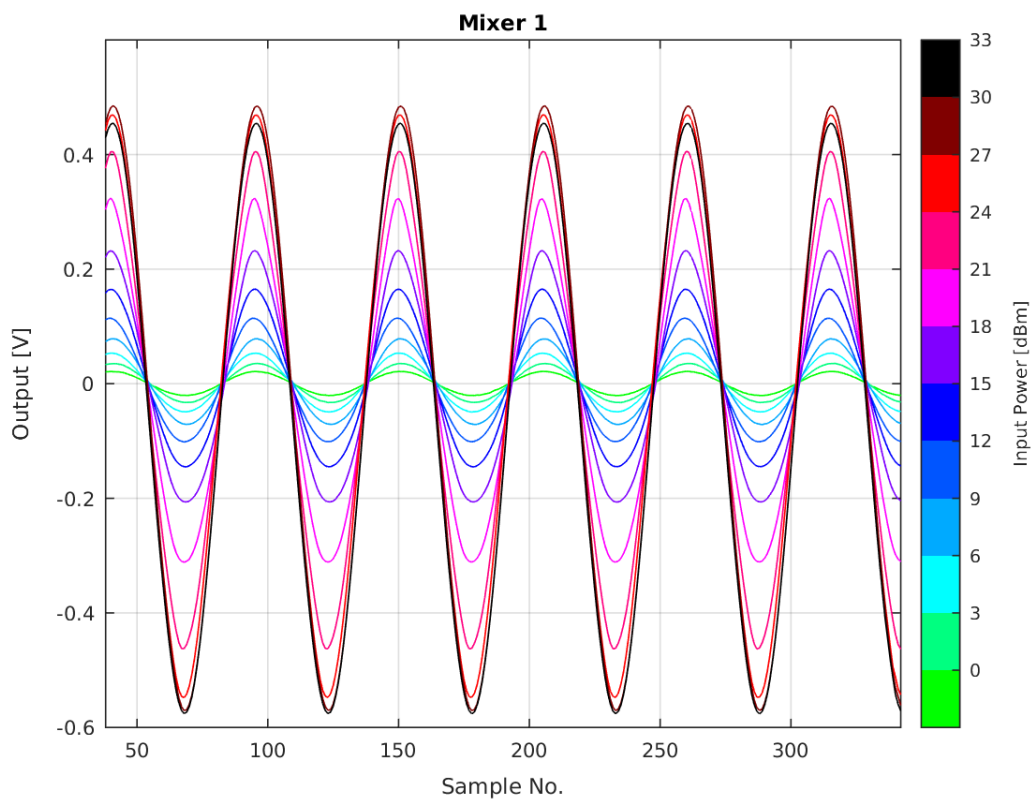


Figure 1.10: Response of Mixer 1 to signal generator input.

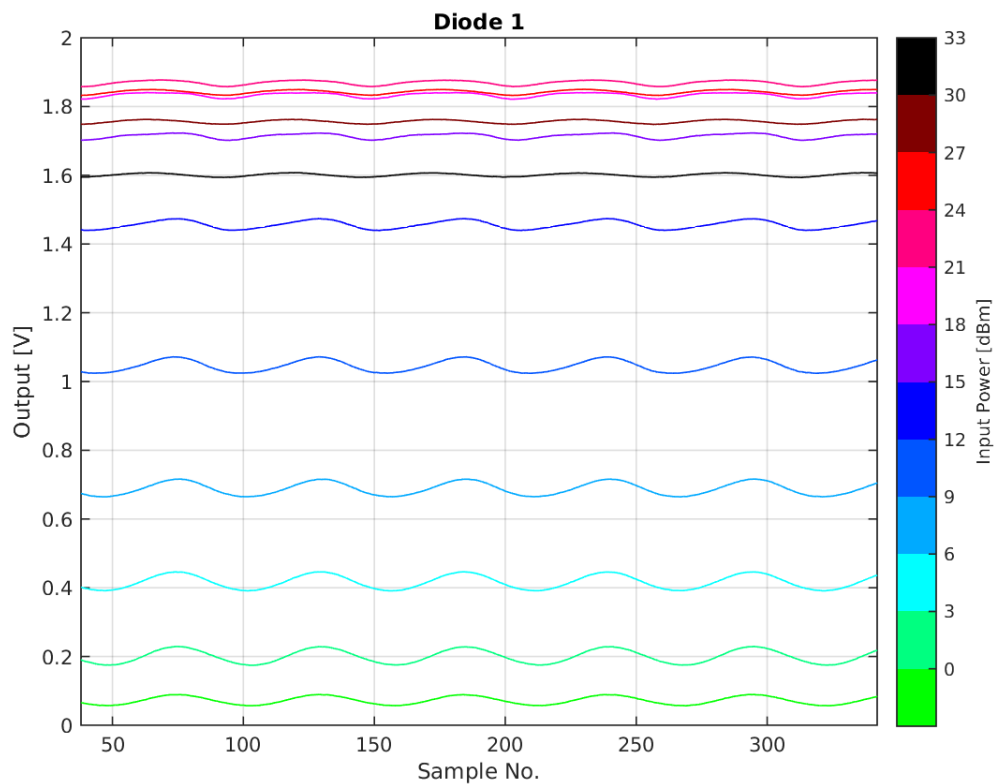


Figure 1.11: Response of Diode 1 to signal generator input.

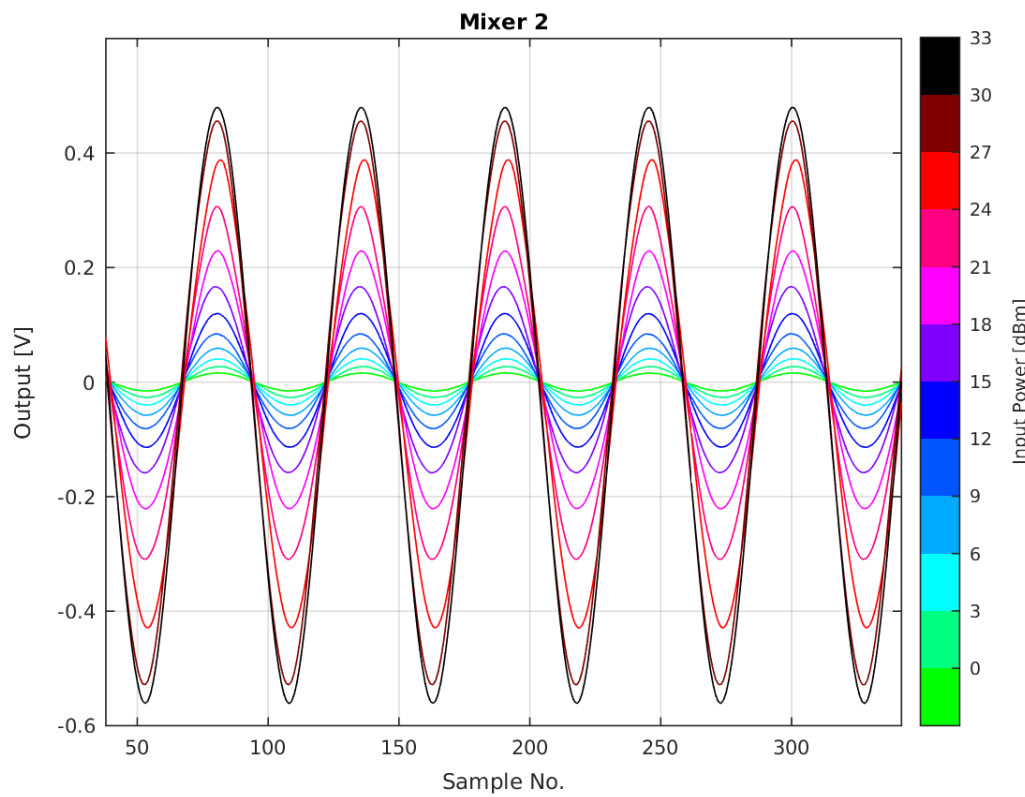


Figure 1.12: Response of Mixer 2 to signal generator input.

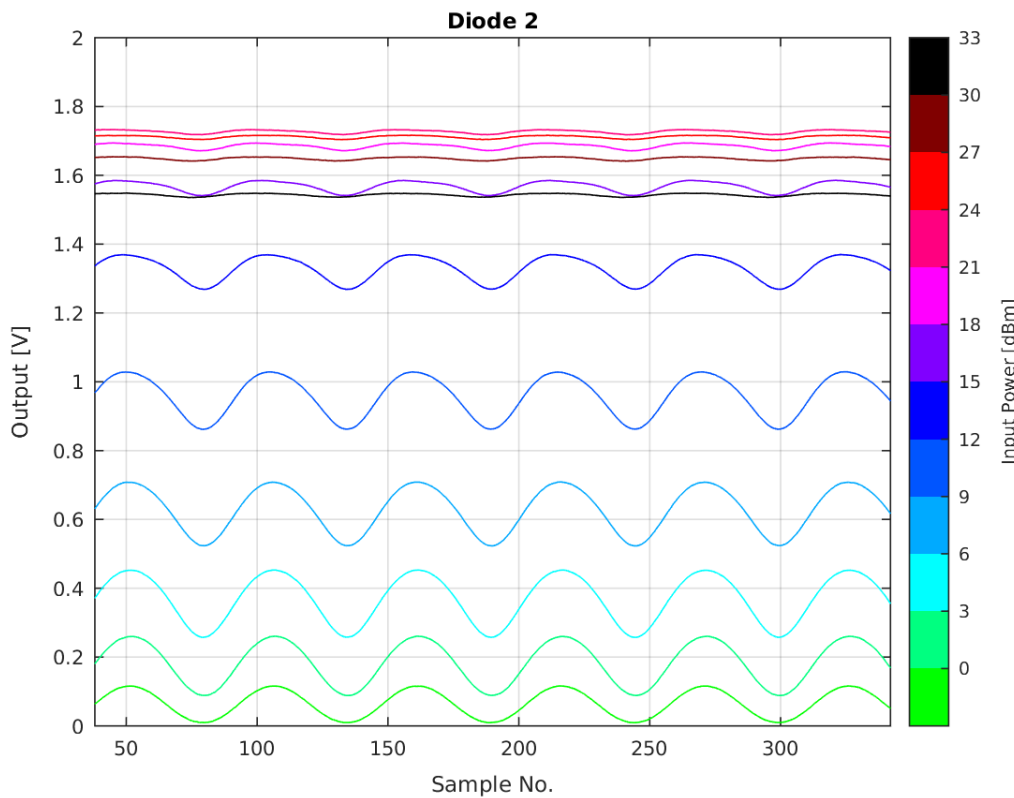


Figure 1.13: Response of Diode 2 to signal generator input.

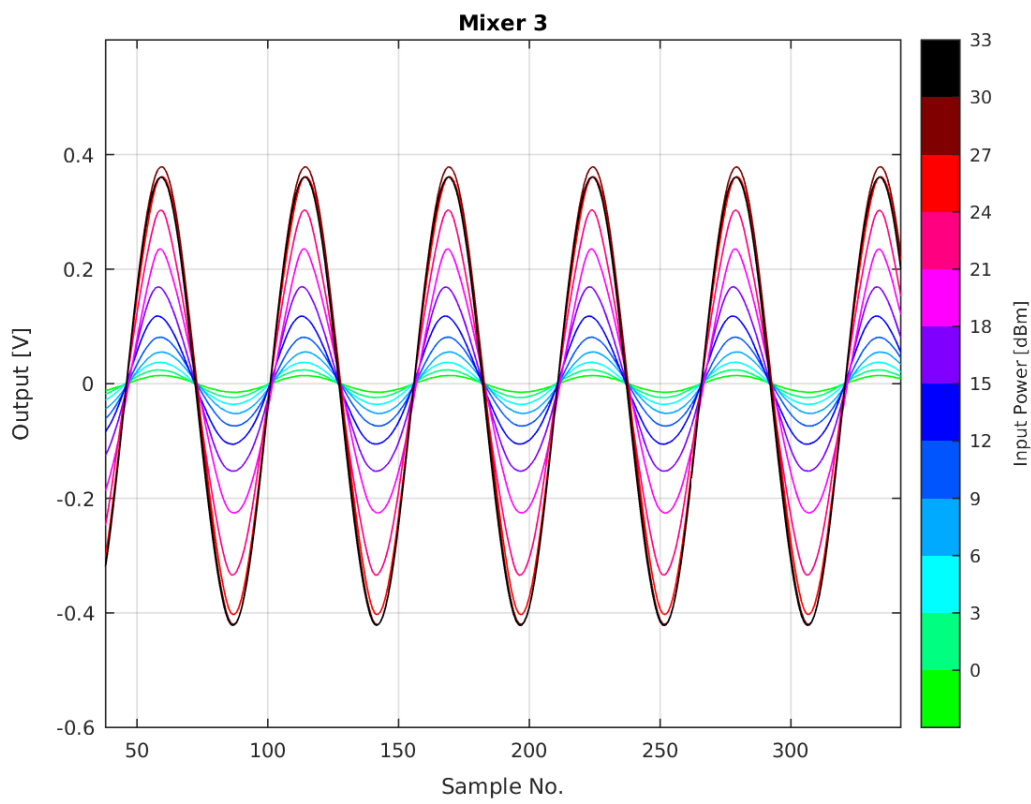


Figure 1.14: Response of Mixer 3 to signal generator input.

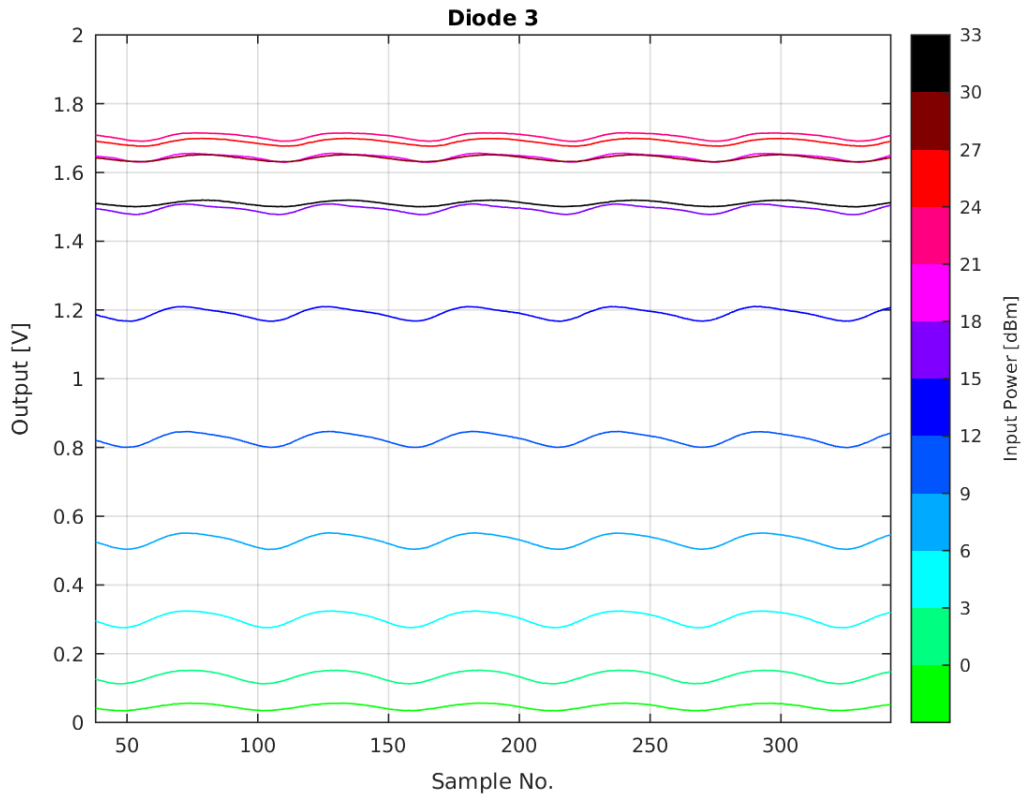


Figure 1.15: Response of Diode 3 to signal generator input.

only a slight **oscillation** about the ideal sinusoidal behaviour. The deviation from ideal is at the level of  $0.25 \pm 0.03^\circ$  and  $0.30 \pm 0.04^\circ$  for the first and third mixers, with a slightly larger effect of  $0.45 \pm 0.04^\circ$  for the second mixer. This applies within  $\pm 80^\circ$  of the zero crossing in the mixer output. Within  $\pm 10^\circ$  of the maximum or minimum output the deviation from the sine fit rapidly increases, reaching several degrees for each mixer. For operation with the beam this means that the accuracy of the phase measurement cannot be guaranteed when the LO phase is set so that the mixer is giving close to its maximum or minimum output. This is also true for other reasons, as seen in Section ???. The PFF system can only correct small offsets at the level of around  $\pm 5^\circ$  (Section ??), so the non-ideal response close to peak output is not an issue for the PFF performance.

However, for input powers in the range from 15–21 dBm the non-ideal characteristics of the mixers are larger. One example of this is shown in Figure 1.18, at an input power of 18 dBm. If input powers in this range are used calibrations of the mixer response should normally be restricted to around the zero crossing so that the fitted amplitude gives the best approximation to the true behaviour for small phase offsets.

## Dependence on Input Power

The mixer output is expected to **linearly depend** on the input voltage and the diode on the square of the input voltage. Both these dependencies must hold in order to use Equation 1.12 and obtain a phase measurement that does not depend on the input voltage to the electronics (therefore making the calculated phase insensitive to any possible variations in power along the pulse from the beam signal, for example). For these measurements the input voltage can be calculated using the known input power and  $50\ \Omega$  impedance of the electronics.

Figure 1.19 shows the dependence of the mixer output amplitudes on the input voltage. As seen previously the first mixer gives a larger output than the other two mixers. The 2nd and 3rd mixers give a similar response up to an input voltage of 3.5 V (24 dBm). Dashed lines in the figure show a linear fit to the mixer output restricted to the range between 0.45 V and 1.75 V (6 dBm to 18 dBm) in each case, as marked by the vertical black lines. All three mixers give a linear response up to an input voltage of around 3 V (23 dBm), after which the effects of saturation begin to appear. By an input voltage of 5 V (27 dBm) the first and third mixers are almost fully saturated with almost no remaining power dependence in the output. The second mixer begins to enter saturation at the same voltage as the other two mixers but retains a strong power dependence up to a higher input voltage of 7 V (30 dBm).

## Asymmetry in Output

One final interesting property of the mixers is that the output is not symmetric about zero, in other words the maximum output voltage is different to the absolute value of the minimum output voltage. This is perhaps most visible looking back to the Mixer 1 output at all power levels in Figure 1.10, where the maximum output is around +0.45 V but the minimum output is around -0.55 V.

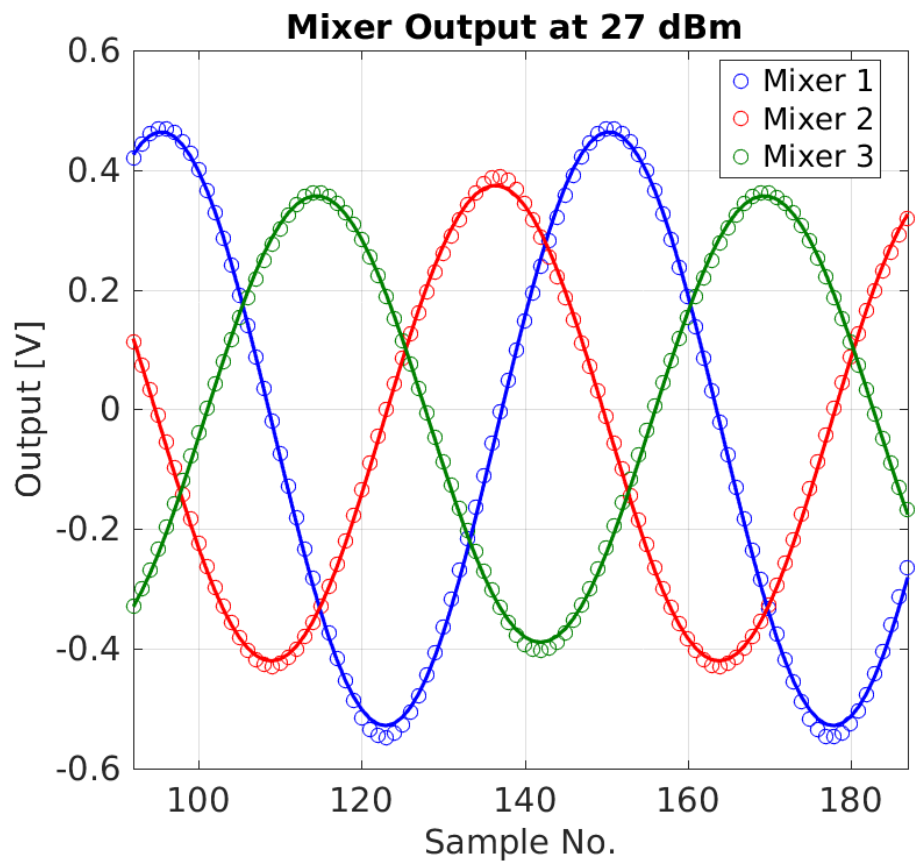


Figure 1.16: Sinusoidal fit to mixer responses at 27 dBm input power.

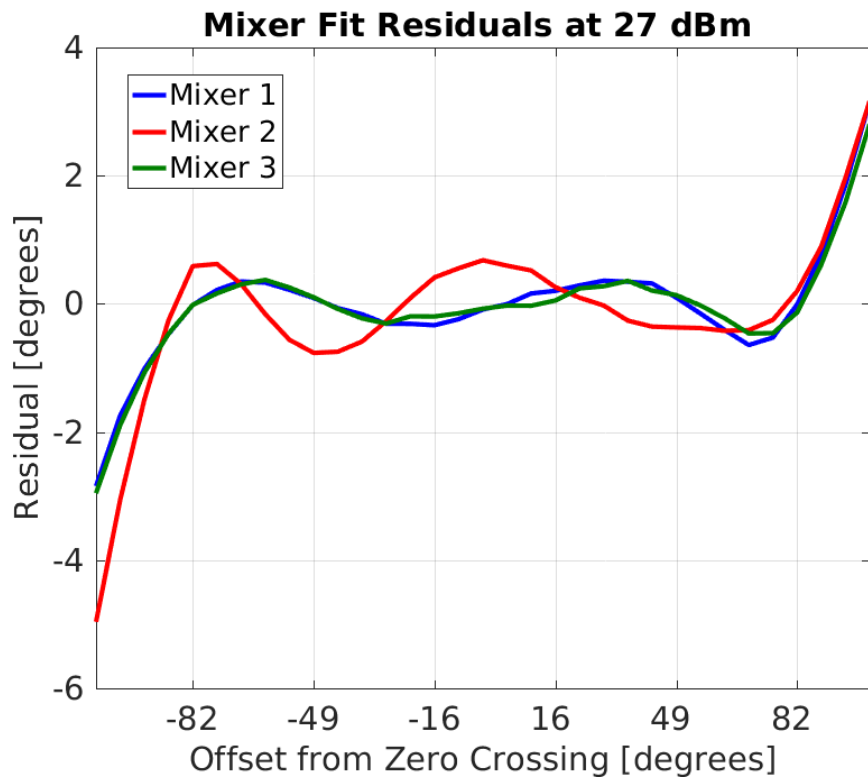


Figure 1.17: Residuals to sinusoidal fit at 27dBm.

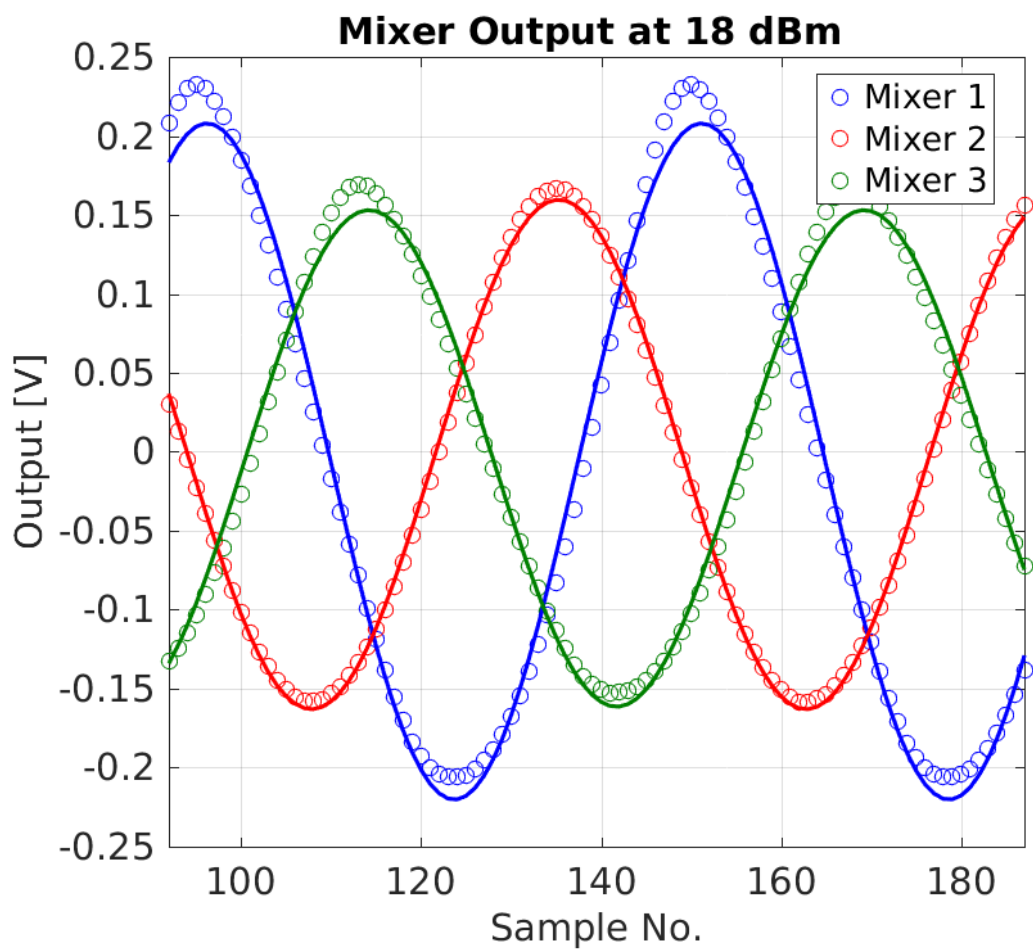


Figure 1.18: Sinusoidal fit to mixer responses at 18 dBm input power.

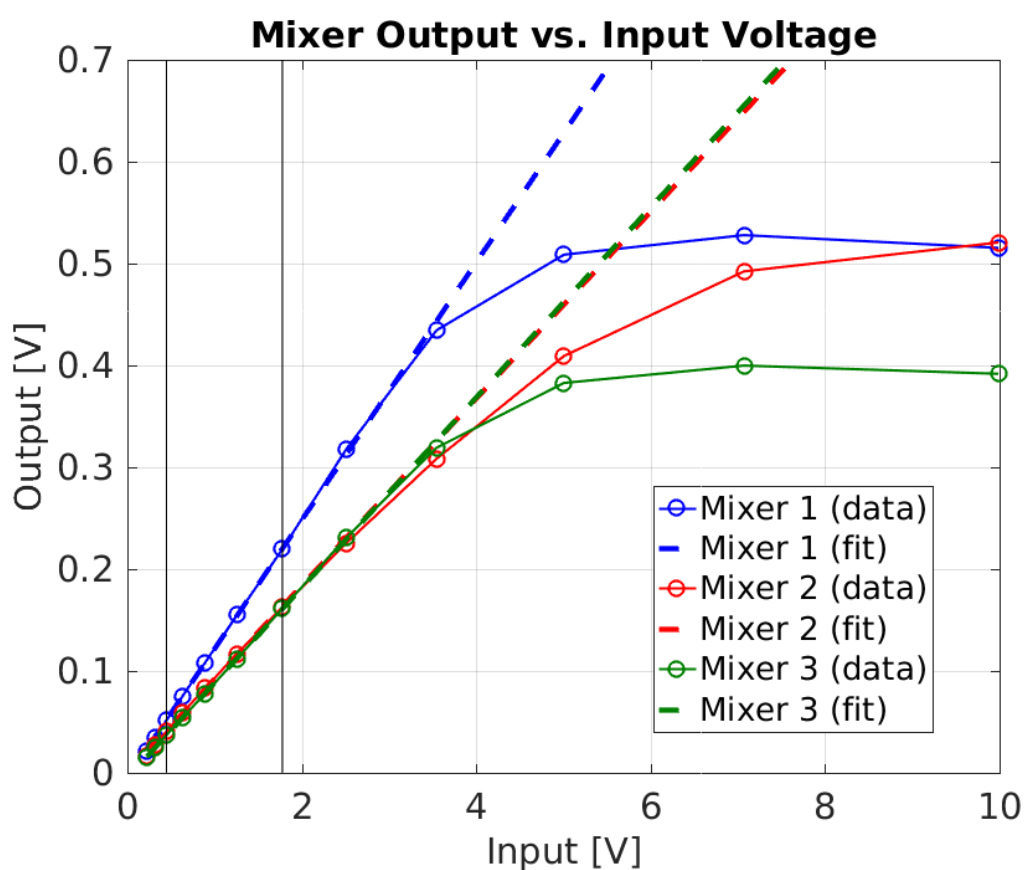


Figure 1.19: Linear fit to mixer output voltage vs. input voltage.

Figure 1.20 shows how the mixer amplitude at maximum and minimum output varies with the input voltage. Mixer 1 asymmetry is largest for Mixer 1 and smallest for Mixer 3. The effect appears to increase in magnitude with the input voltage, with the  $\sim 100 \text{ mV}$  difference mentioned previously for Mixer 1 at an input of 10 V, but differences of only several mV at low input powers. For each mixer the amplitude at maximum output is larger for input voltages up to 2.5 V (21 dBm). Above 2.5 V input voltage this flips, with the minimum mixer amplitude being larger than the maximum amplitude.

For input voltages between 0.45 V and 1.25 V (6 dBm to 15 dBm) the mixer asymmetry has an approximate quadratic dependence on the input voltage, as shown in Figure 1.21. Outside this range there is no simple relationship that can explain the dependence of the asymmetry on the input voltage. One explanation for the asymmetry in the mixer outputs is cross-talk coming from the diode signals. Above 15 dBm the diodes enter saturation, as discussed in the next section, which may explain why the quadratic fit to the mixer asymmetry is only valid at power levels up to this value.

Taking the power dependent asymmetry into account the actual mixer response can be modified from Equation 1.9 to become:

$$\text{Mixer}(t) = m_1 A(t) \sin[\phi(t)] + m_2 A(t)^2 + m_3 A(t) + m_4 \quad (1.33)$$

Where  $A(t)$  is the input voltage at time  $t$ , and  $m_1, m_2, m_3$ , and  $m_4$  are calibration constants.

## 1.6.4 Diode Performance

### Dependence on Input Power

The dependence of the three diode outputs on the input power is shown in Figure 1.22, with the square root of the diode output plotted rather than the diode directly as this is the expected linear relationship. Immediately it is apparent that the diode signals saturate at much lower input voltages than the mixer signals. All three diodes are almost fully saturated at an input of 2 V (20 dBm), with the effects of saturation already beginning to appear above 1.25 V (15 dBm). Figure 1.23 shows a linear fit to the square root of the diode, using the range of input voltages between 0.45 V and 1.25 V (6–15 dBm). Even below saturation the response of  $\text{sqrt}(\text{Diode})$  is not well approximated by a linear dependence as desired. However, in the range from 0.30 V to 1.25 V (3 dBm to 15 dBm) a quadratic fit to the diode output directly (not  $\text{sqrt}(\text{Diode})$ ) does give a good approximation to the true dependence of the diodes on the input voltage. This is shown in Figure 1.24.

### Cross-Talk

As seen previously in Figures 1.11, 1.13 and 1.15 the diode outputs show a sinusoidal oscillation. Like there is cross-talk from the diode on the mixer outputs, there is also cross-talk from the mixers on the diode outputs. Figure 1.25 shows a sinusoidal fit to the cross-talk on Diode 1 at an input power of 6 dBm. It has the same characteristics as the mixer output, including the slight distortion away from ideal sinusoidal behaviour around the peaks.

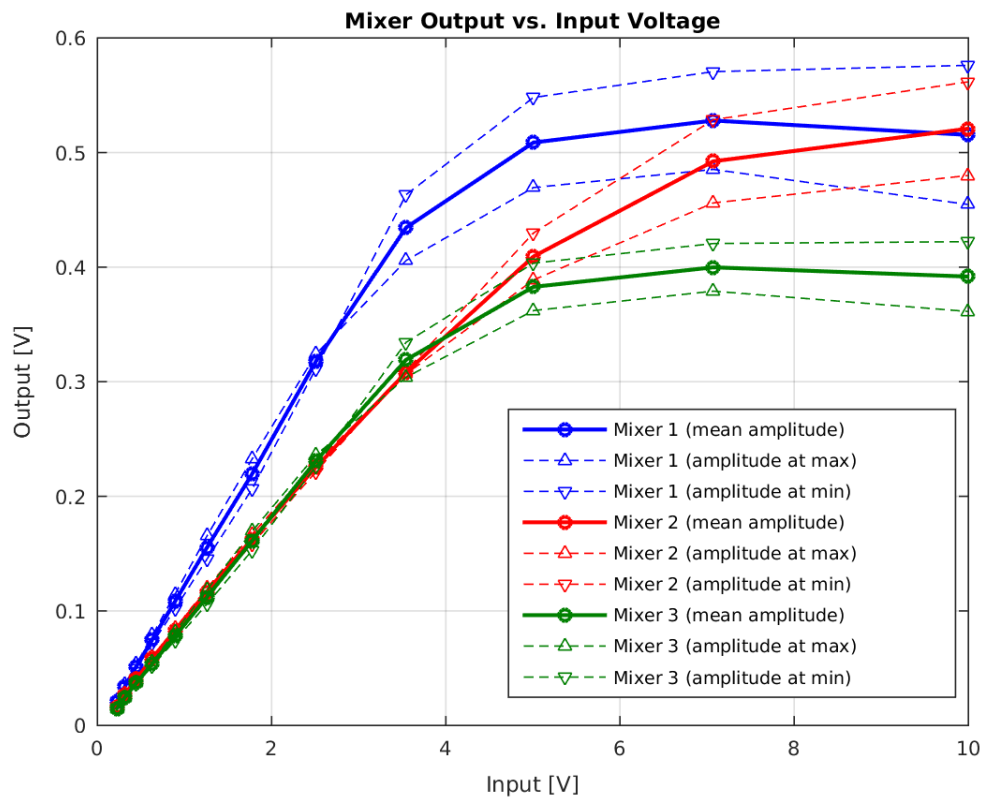


Figure 1.20: Mixer maximum and minimum output voltage vs. input voltage.

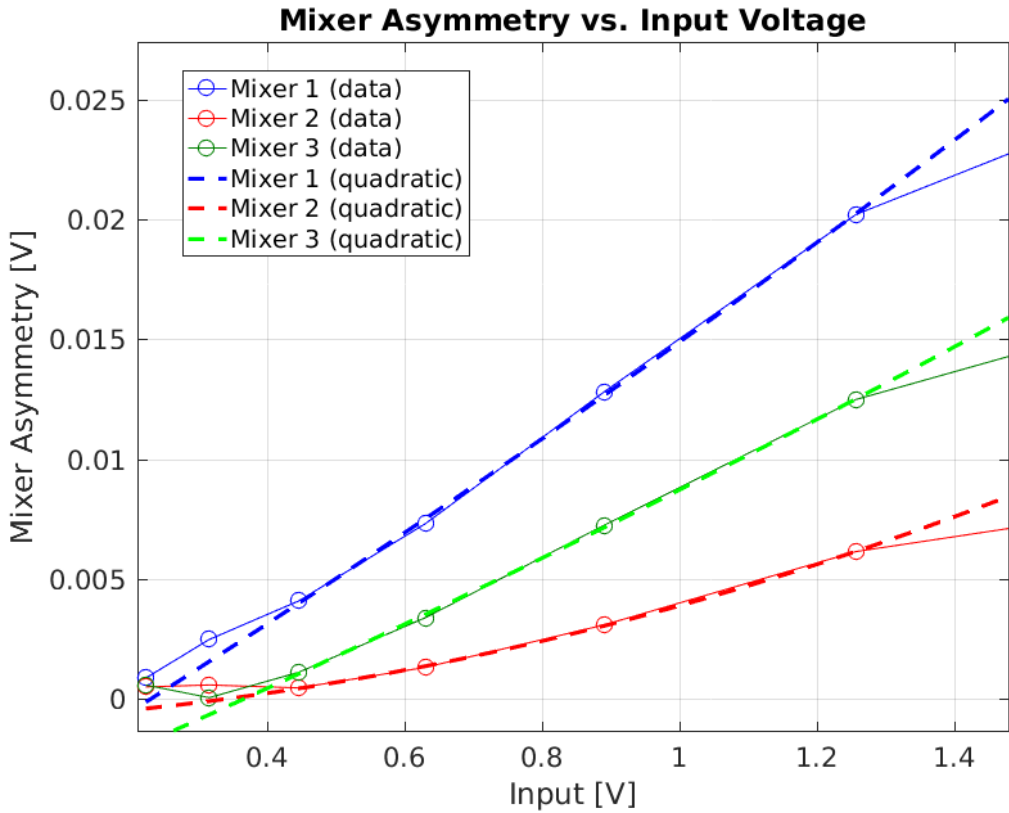


Figure 1.21: Relative amplitude vs. input power of cross-talk on the mixer from the diode.

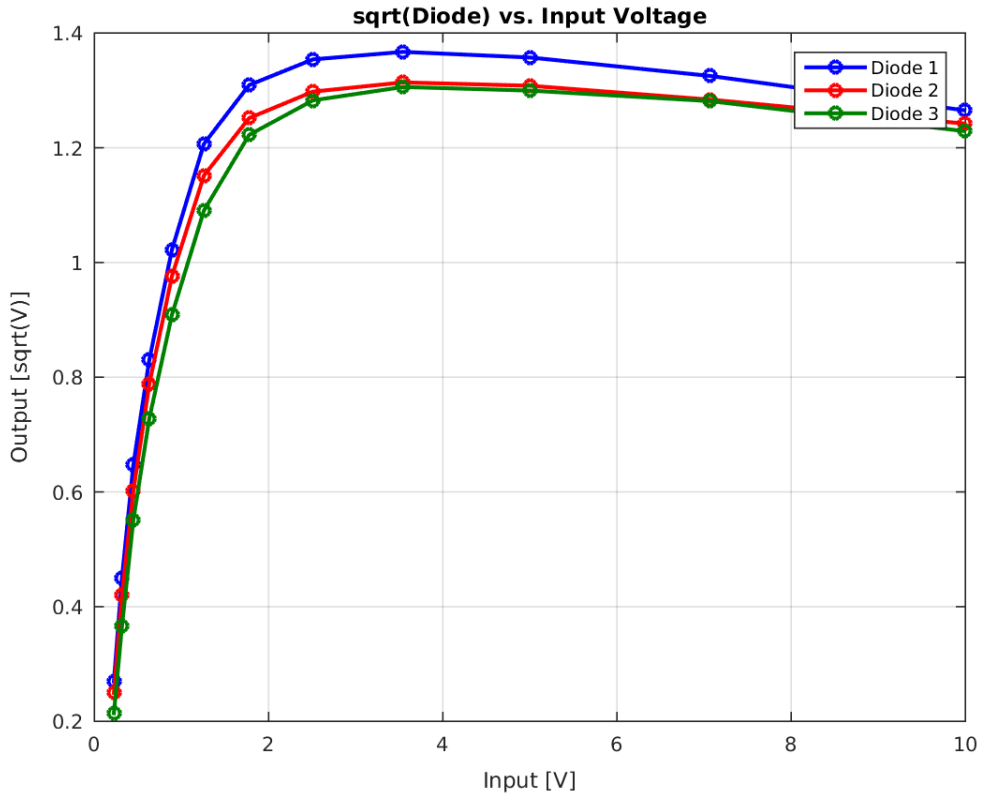


Figure 1.22:  $\text{sqrt}(\text{Diode})$  vs. input voltage.

However, as the diodes enter saturation the oscillation is initially distorted, and then has a much smaller amplitude when the diode output is fully saturated. One example of this is shown for the Diode 1 output at 18 dBm in Figure 1.26. The peaks around the maximum output are clearly non-sinusoidal in this case.

Figure 1.27 shows the dependence of the relative amplitude of the cross-talk on the input power. The relative amplitude of the cross-talk means the fitted amplitude of the sinusoidal oscillation on the diode divided by the mean diode output. Up until the diode outputs are fully saturated the relative amplitude of the cross-talk is around a factor two larger for the second diode. For example, at an input power of 12 dBm the relative cross-talk is at around the level of 30% for the second diode, or 15% for the first and third diode outputs. Up to input powers of 15 dBm the relative cross-talk is always above 10%.

Finally, Figure 1.28 compares the oscillation on the diode to the oscillation on the mixer. It can be seen that there is a phase shift between the two, which adds a further complication to the necessary phase reconstruction method. Taking in to account the actual characteristics of the diodes, including the cross-talk and quadratic dependence on the input power, the expected expression for the diode output from Equation 1.10 can be modified to:

$$\text{Diode}(t) = d_1 A(t)^2 + d_2 A + d_3 + d_4 A(t) \sin[\phi(t) + \delta] \quad (1.34)$$

Where  $d_1, d_2, d_3, d_4$  and  $\delta$  are calibration constants.

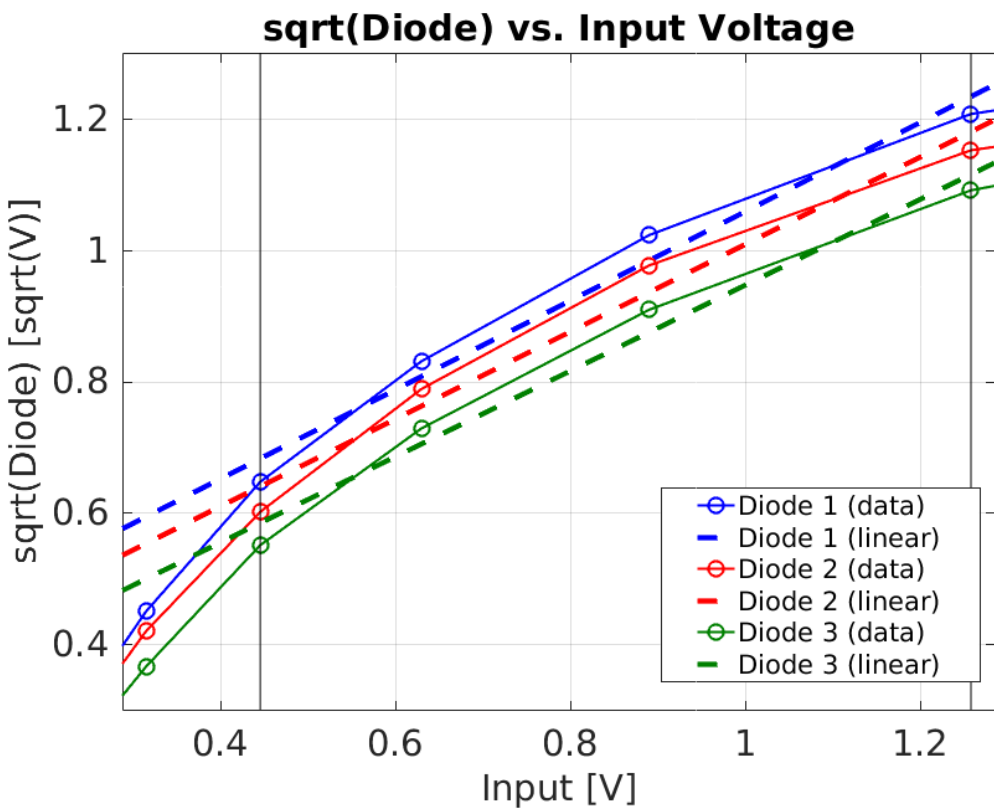
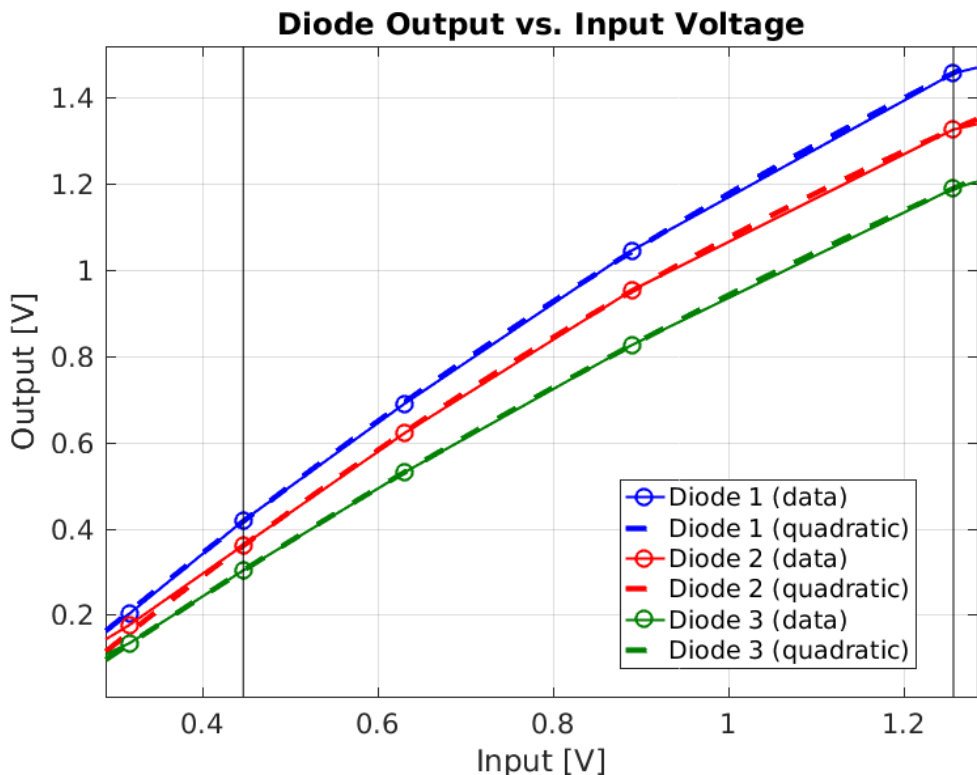
Figure 1.23: Linear fits to  $\text{sqrt}(\text{Diode})$  vs. input voltage.

Figure 1.24: Quadratic fits to Diode vs. input voltage.

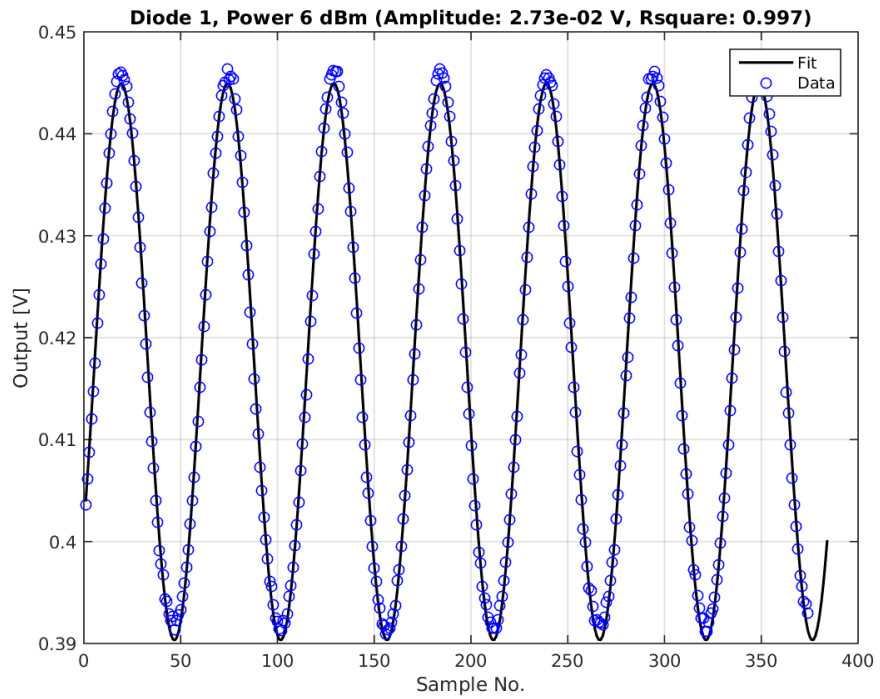


Figure 1.25: Sinusoidal fit to cross-talk on diode at 6 dBm input power.

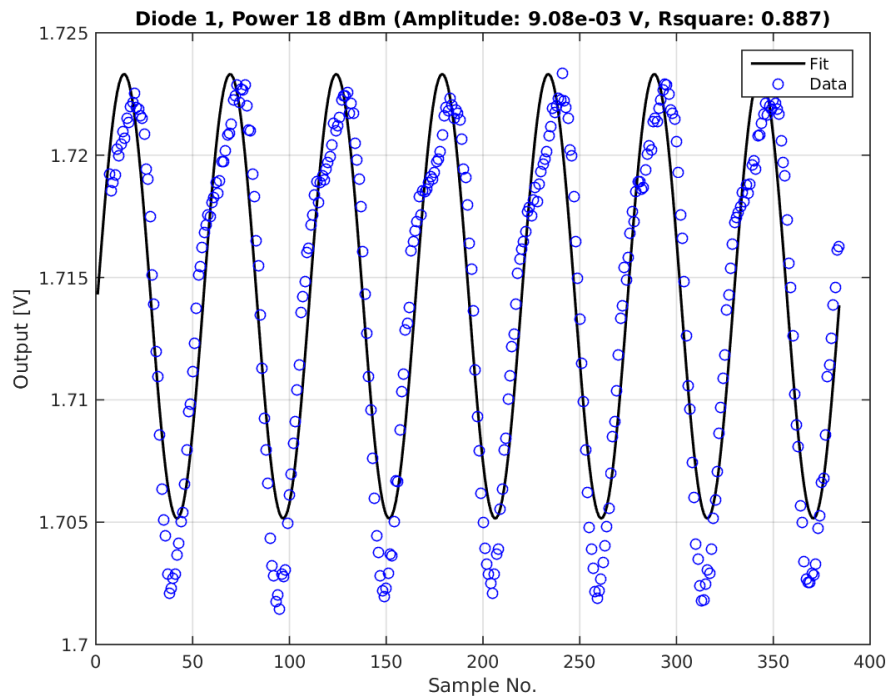


Figure 1.26: Sinusoidal fit to cross-talk on diode at 18 dBm input power.

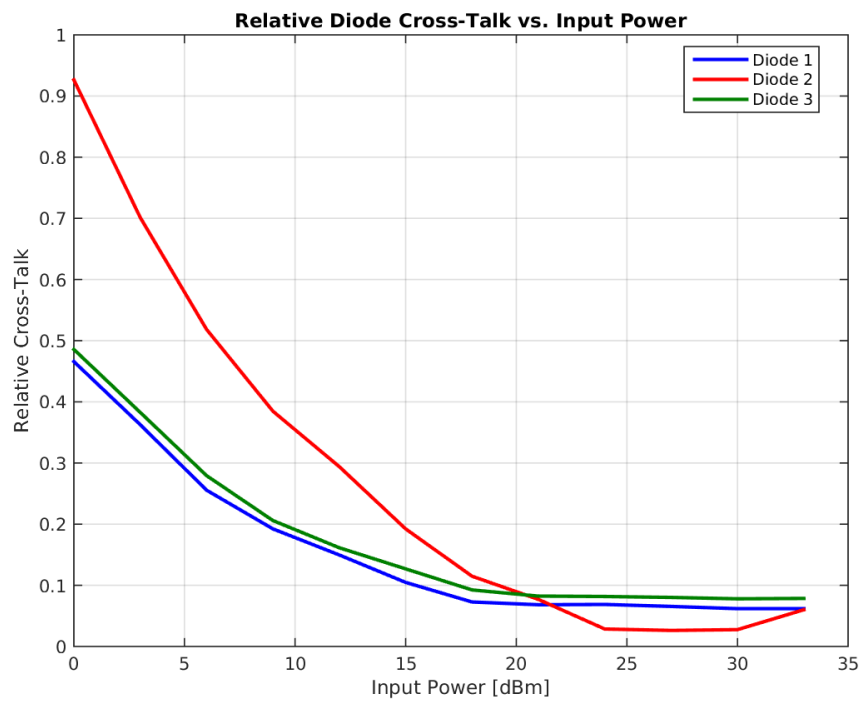


Figure 1.27: Dependence of the relative amplitude of cross-talk on the diode versus the input power.

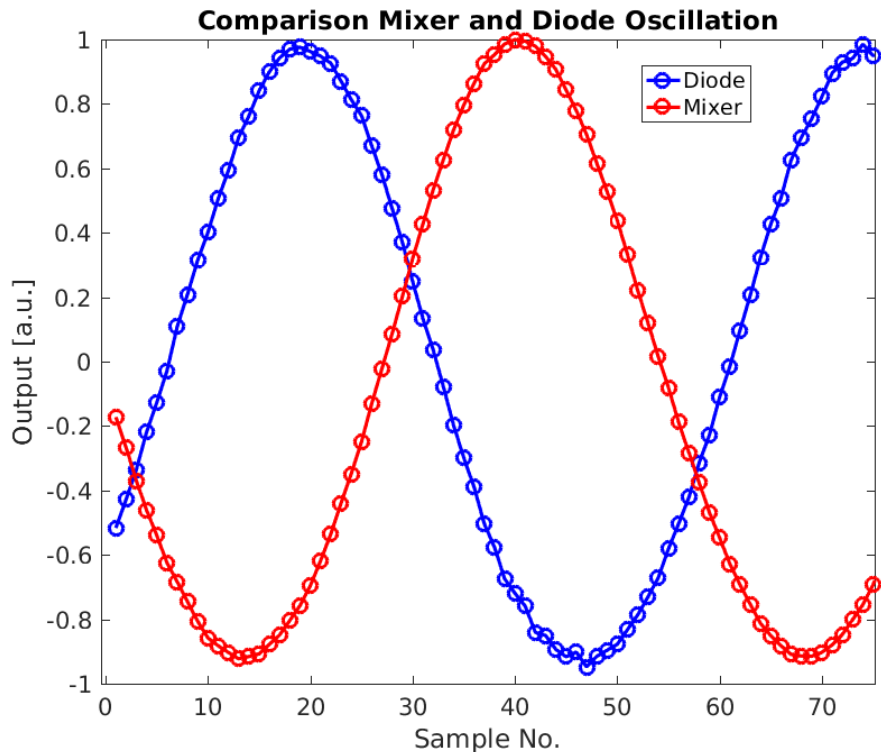


Figure 1.28: Comparison of the oscillation on the mixer and the diode, showing a relative phase offset between the two.

### 1.6.5 Consequences for Normal Operation

The results of the signal generator tests have several consequences for the setup of the electronics and phase reconstruction during normal operation with the beam induced signals from the phase monitors. Firstly, in order to maximise the signal to noise ratio and yield the best possible resolution on the phase measurement the highest possible input power below saturation should normally be used. The degradation of the phase resolution with the input power is seen for beam based measurements in [Section \[REF\]](#). However, the diodes begin to enter saturation much earlier than the mixers, at around 15 dBm rather than 23 dBm. This means that in order to be able to use the diode measurement as part of the phase reconstruction the input power would have to be limited to below 15 dBm, 8 dBm lower than would be ideal for the mixer performance. There is no way to use different input powers for the mixers and diodes without a complete redesign of the electronics.

Secondly, the modifications that the cross-talk on the mixer and diode make [to](#) Equations 1.33 and 1.34 above makes the needed calculation to reconstruct the phase much more complex than the ideal case using Mixer/sqrt(Diode) in Equation 1.12. In particular, the dependence of the diode output on  $\sin(\phi + \delta)$  means there is no simple expression that can be derived to create an input power independent phase measurement. An iterative process would have to be used to estimate the phase instead, converging towards the true diode output without cross-talk after each iteration using the estimated phase value. This may be possible in offline data analysis but would be difficult to implement in the PFF algorithm whilst still meeting latency requirements.

Due to these reasons, and with no possibility to make modifications to the electronics, the decision was eventually taken to not include the diode measurement in the [phase reconstruction process](#). For operation with the beam this means making the assumption that the output power from the phase monitors is constant along the pulse, and that the jitter in the output power is small. This is a good approximation, as seen later in [Section \[REF\]](#). To reduce the sensitivity to any slow drifts in the output power due to changes in the beam conditions calibrations are taken at regular intervals between measurements.

[With this treatment](#) of the electronics [outputs](#) the phase is reconstructed as follows:

$$\text{Mixer}(t) = A \sin[\phi(t)] + d \quad (1.35)$$

$$\phi(t) = \arcsin\left(\frac{\text{Mixer}(t) - d}{A}\right) \quad (1.36)$$

Two calibration constants are needed –  $A$  and  $d$ .  $A$  is the fitted amplitude of the sinusoidal mixer output, and  $d$  is the asymmetry or offset between the maximum and minimum mixer output. This is a simplified form of Equation 1.33 given the assumption that the power is constant. In reality both  $A$  and  $d$  have a power dependence.

As any variations in input power are not removed by this method there is a benefit to operating the mixer in a region where the power dependence of the output is reduced. The best phase resolution achieved to date has been achieved with input powers to the electronics in the range between 24.5 dBm and 27 dBm (as stated in [\[REF\]](#)), [where the mixers have actually begun to enter saturation, as a result](#). Operating in this range also has the benefit

of reducing the deviation from ideal sinusoidal behaviour at lower input powers as seen in Section 1.6.3.

All the beam based measurements in the remainder of this chapter and the rest of the thesis use this phase reconstruction approach. Although the diodes are no longer directly used as part of the phase measurement they are still useful for the purposes of the time alignment of signals and for monitoring whether there have been any large changes in input power. The PFF firmware on the FONT5a feedforward controller has also been changed to add the option to not include the diode in the correction calculation (Section ??). The nominal PFF setup, as used for the results presented in Chapter ??, now does not use diode normalisation.

## 1.7 Calibrations

The remainder of this chapter presents the performance of the complete phase monitor and electronics system for normal operation with the beam, replacing the signal generator with the RF output from the phase monitors.

The first step in using the phase monitor measurements is to calibrate the mixer outputs. Calibrations of the phase monitor signals are typically taken on a daily basis during data taking periods, as well as additional calibrations when there have been any changes in beam conditions or to the setup of the electronics. These are needed to determine the calibration constants, amplitude and offset, to be able to determine the phase from the mixer output as previously discussed. This section presents typical calibration results for all three phase monitors and discusses aspects such as the stability of the calibration along the pulse and determining the optimal set point for the LO phase shifters.

For beam based measurements calibrations are performed using the LO phase shifters. By varying the LO phase shifter the phase between the LO and the beam signal is changed. During a calibration the phase shifters are moved through  $360^\circ$  at 12 GHz so that the response of the mixer to all phase offsets between the beam and LO can be determined. Normally calibrations are taken at 12 shifter settings across the full  $360^\circ$  range, with 10 pulses acquired at each setting and the whole scan taking approximately 10 minutes. These choices are a compromise between having enough points for a good quality fit whilst reducing the possibility of large drifts in beam phase during the scan which would degrade the fit results. All the calibrations presented use the electronics setup with the mechanical LO phase shifters in place (Section 1.8). The settings on these phase shifters approximately correspond to degrees at 4 GHz, thus a phase shifter change of 120 units corresponds to  $360^\circ$  at 12 GHz.

A calibration from both the SiS digitiser and FONT5a setup will be shown. During operation of the PFF system Mon 1 is usually connected to the FONT5a board as the correction input, whilst Mon 2 and Mon 3 are connected to the SiS digitisers where they can be acquired together with other signals at CTF3. The difference in measured output voltage between the two setups results from the use of an amplifier before the SiS digitisers to reduce

noise in that setup (Section 1.4). Also, when using the FONT5a board the mixer outputs are attenuated by 1 dB to avoid saturating the FONT ADCs. The calibration constants from Mon 1 on the FONT5a board are needed for the PFF gain calculation in Section ???. All measurements of the upstream and downstream phase after this chapter use Mon 2 and Mon 3 on the SiS digitisers and their respective calibration constants.

### 1.7.1 Calibration on SiS Digitisers

Figures 1.29–1.31 show the output of the mixer for each phase monitor along the pulse for all the phase shifter settings used during the LO scan. Away from the minimum and maximum output each mixer shows the expected phase sag along the beam pulse resulting from the RF pulse compression used at CTF3 [REF]. The shape of the phase sag as seen on the mixer changes sign depending on whether the LO phase places the mixer on the rising or falling slope of its sinusoidal output. Usually the mixers are operated on the falling slope where the measured phase sag is ‘u’-shaped, rather than ‘n’-shaped, as this is also the convention for other phase dependent signals at CTF3 [REF].

Near the minimum or maximum mixer amplitude the beam phase sag causes a much smaller variation in the mixer output voltage along the pulse. The phase resolution close to the peaks in the mixer output is therefore greatly reduced, as seen in Section ???. LO phase scans are used to not only calculate the calibration constants but also to determine the phase shifter settings that zero the mixer output, where the resolution is maximal. This process is documented in Section 1.7.4.

The noisier appearance of the output on Mon 3 is not an effect of the phase monitors or phase monitor electronics but is rather caused by real differences between the beam phase upstream (Mon 1, Mon 2) and downstream (Mon 3). Reducing the differences between the upstream and downstream phase is the focus of Chapter ??.

Figure 1.32 shows the result of fitting the mixer output versus the phase shifter setting at sample 605 along the pulse. The mixer response is sinusoidal as expected and as seen previously in the signal generator tests. In the signal generator tests there was some visible distortion away from the sine fit around the peaks at some input power levels (Section 1.6.3). There is no visible effect at the powers of the phase monitor signals (Section 1.1). Differences in the peak output of each monitor are expected due to differences in the input power from each phase monitor as well as differences between the sets of electronics. Small offsets between the data and the fit at some shifter settings are caused by drifts in the beam phase during the scan (particularly for Mon 3 where the beam is less stable), as well as human error in setting the shifter values.

The fitted values of the mixer amplitude,  $A$ , and offset,  $d$ , are found in Table 1.6. These values are used to calculate the beam phase as per Equation 1.36.

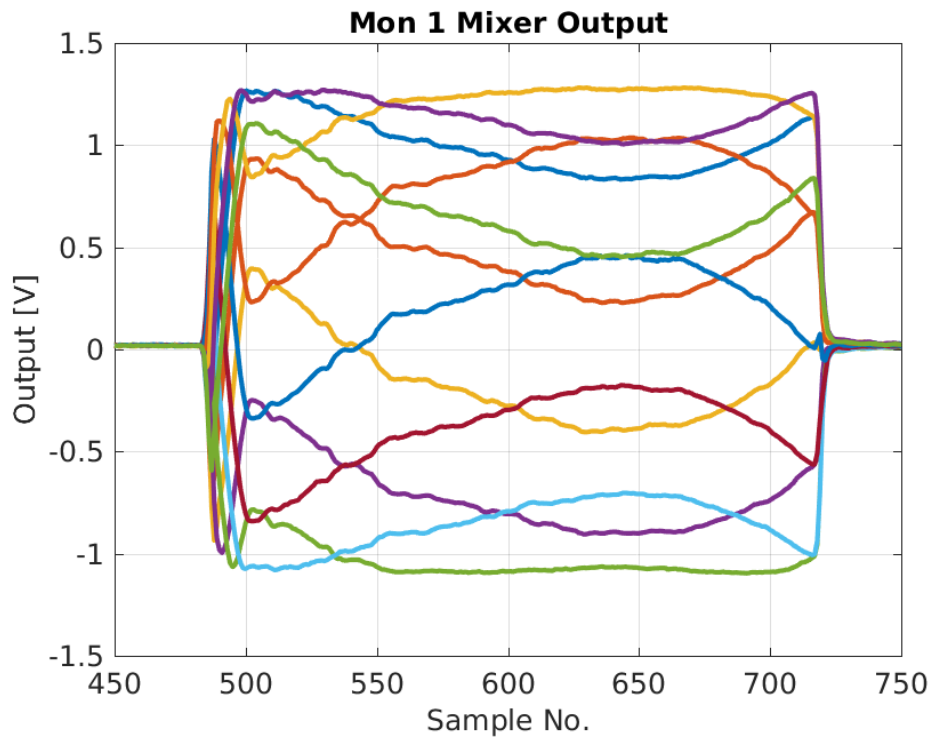


Figure 1.29: Mon 1 phase along the pulse for each LO phase shifter setting during the calibration.

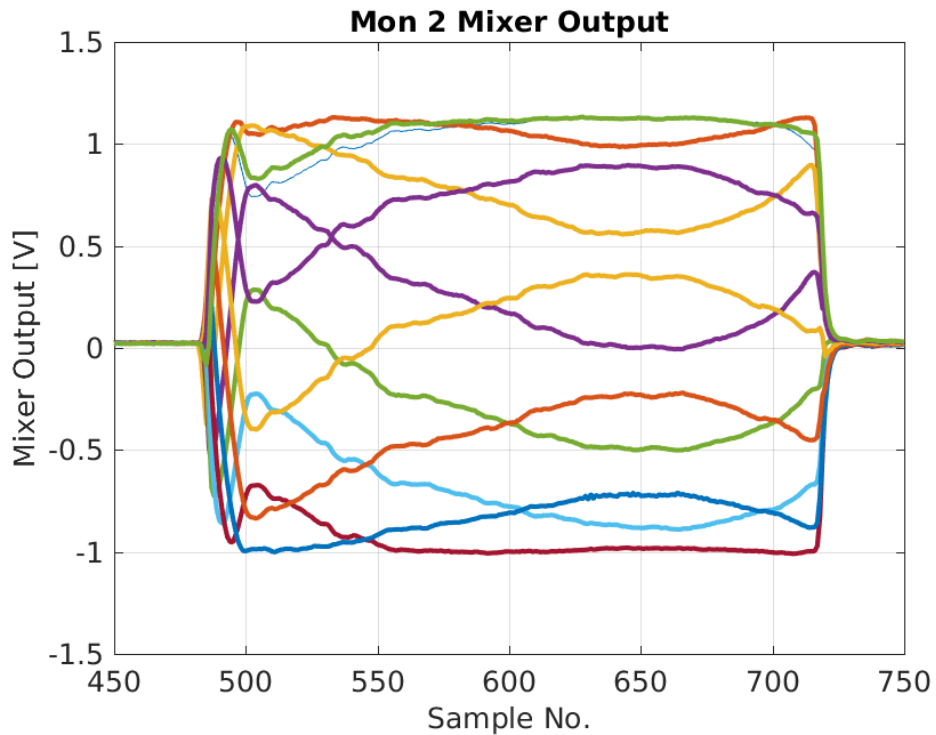


Figure 1.30: Mon 2 phase along the pulse for each LO phase shifter setting during the calibration.

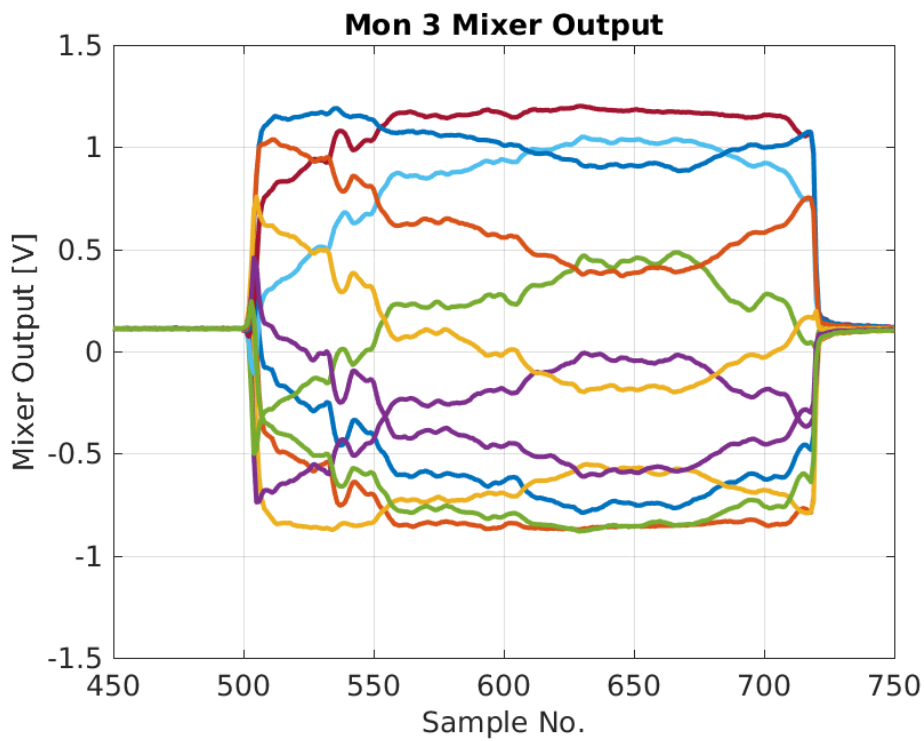


Figure 1.31: Mon 3 phase along the pulse for each LO phase shifter setting during the calibration.

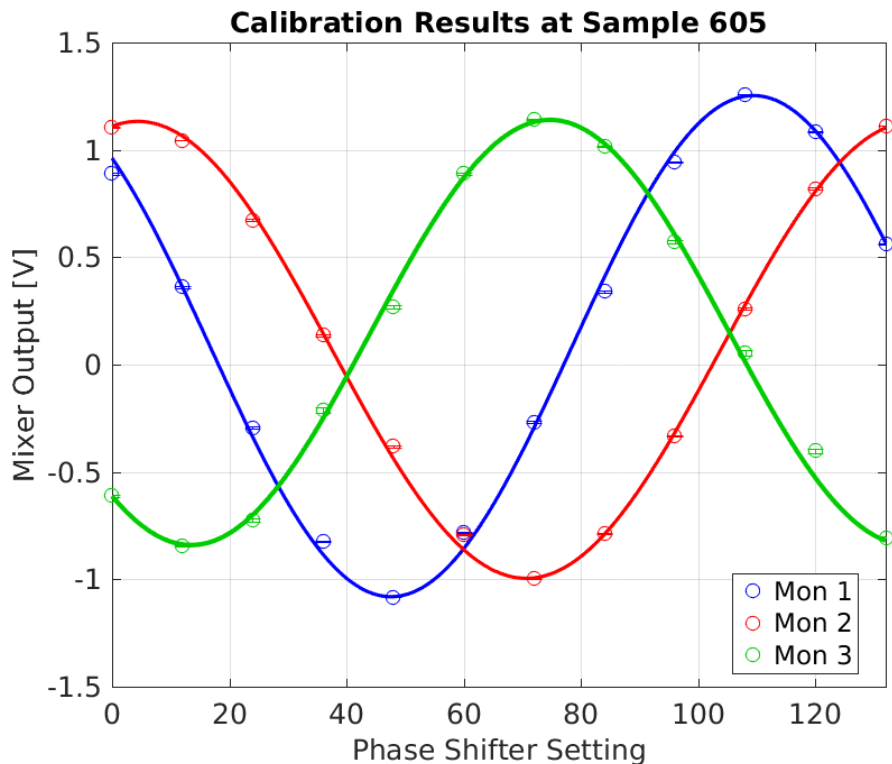


Figure 1.32: Fits to the mixer output vs. LO phase shifter setting at sample 605 on the SiS digitisers.

Monitor	$A$ (amplitude)	$d$ (offset)
Mon 1	$1167 \pm 10$ mV	$86 \pm 9$ mV
Mon 2	$1064 \pm 6$ mV	$69 \pm 7$ mV
Mon 3	$990 \pm 12$ mV	$150 \pm 10$ mV

Table 1.6: Fit parameters from the calibration on the SiS digitisers for each monitor.

Monitor	$A$ (amplitude)	$d$ (offset)
Mon 1	$3434 \pm 41$ counts	$-278 \pm 34$ counts
Mon 2	$3144 \pm 16$ counts	$-138 \pm 17$ counts
Mon 3	$2870 \pm 43$ counts	$-44 \pm 44$ counts

Table 1.7: Fit parameters from the calibration for each monitor on the FONT5a board.

## 1.7.2 Calibration on FONT5a Board

Figure 1.33 and Table 1.7 show the results of a calibration performed in exactly the same way but on the FONT5a board. The FONT5a board ADCs flip the sign of the input [REF], so a positive ADC output in counts corresponds to a negative input voltage and vice-versa. This explains why the apparent mixer output is on the **rising slope at a phase shifter setting of zero on the FONT5a board in Figure 1.33**, but on the falling slope on the SiS digitisers in Figure 1.32. For operation of the PFF system this difference must be taken in to account either by operating the mixer on the rising slope as seen on the FONT5a board (which in reality is the falling slope, as desired), or alternatively by using negative gain values for the correction output. The fitted values for  $d$  in Table 1.7 are also negative rather than positive as a result of this sign flip. Apart from these differences the overall shape of the mixer output follows the sinusoidal dependence as expected.

The FONT5a ADC outputs are 13-bit, or  $\pm 4096$  counts, with an input range of  $\pm 500$  mV (Section ??). The fitted Mon 1 output, with 1 dB attenuation added after the mixer, of between -3712 counts and +3156 counts therefore corresponds to an input voltage range of between +453 mV and -385 mV. Without the attenuator, which reduces the voltage by roughly 10%, the Mon 1 mixer would saturate the ADC at its peak output. As the contribution of digitiser noise is small on the FONT5a board (Section 1.4) a 1 dB attenuator is also added to the Mon 2 and Mon 3 outputs so that the overall setup for each monitor is the same in this measurement. However, during normal operation of the PFF system Mon 2 and Mon 3 are connected to the SiS digitisers, with their mixer outputs then being amplified rather than attenuated.

## 1.7.3 Multi-Sample Results

The calibration results on both the SiS digitisers and FONT5a board have been presented at one sample number around the middle of the pulse close to where the phase sag along the pulse is flattest. In this section the variation in the fitted calibration constants along

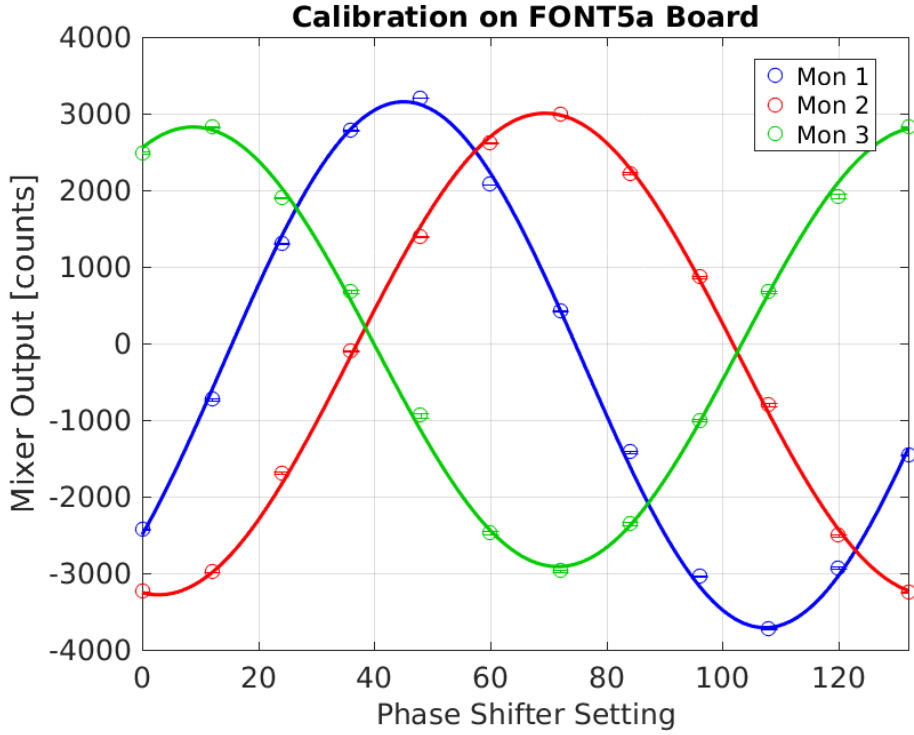


Figure 1.33: Results of a calibration performed on the FONT5a board.

the pulse is discussed. This is particularly important after taking the decision to not use the diodes, as the intended purpose of using the diodes was to normalise the mixer response to give an output independent of the input power. Without using the diodes any variations in input power along the pulse will also create differences in the calibration constants along the pulse.

The current implementation of the PFF algorithm on the FONT5a board uses the mixer multiplied by one gain value that is constant along the full pulse length to create the correction output (Section ??). It therefore cannot take in to account any variations in calibration constants along the pulse. Offline data analysis is usually performed in the same way so that the quoted resolutions are representative of the values that apply to the implementation of the PFF correction. The effect of taking in to account the variations in calibration parameters along the pulse seen here is shown in Section 1.9.2.

Figures 1.34 and 1.35 show the variation in the fitted calibration amplitude and offset across the full pulse length, using the same calibration on the SiS digitisers presented in Section 1.7.1. Differences in both the amplitude and offset along the pulse are visible. These are summarised in Table 1.8 in terms of the standard deviation of the fitted parameter values along the pulse.

The stability of the fitted amplitude along the pulse is similar for the upstream monitors (Mon 1 and Mon 2), with a jitter of around 8 mV in both cases. As the downstream beam is less stable than the upstream beam the variations in fitted ampltitude along the pulse are larger for Mon 3, at the 15 mV level. In terms of a relative difference these values correspond to roughly a 0.7% variation in fitted amplitude for Mon 1 and Mon 2, or 1.5% for Mon 3.

Monitor	$A$ (amplitude)	$d$ (offset)
Mon 1	$8.3 \pm 0.4$ mV	$6.7 \pm 0.3$ mV
Mon 2	$7.7 \pm 0.4$ mV	$3.0 \pm 0.3$ mV
Mon 3	$14.7 \pm 0.7$ mV	$6.1 \pm 0.3$ mV

Table 1.8: Standard deviation in calibration fit parameters along the pulse.

With further optimisation of the downstream beam, as documented in Chapter ??, it should be possible to achieve similar Mon 3 amplitude stability to that seen for Mon 1 and Mon 2.

Absolute stability in the fitted offset along the pulse is similar to that of the amplitude but therefore much larger as a relative difference at the level of several percent. The variation in fitted offset along the pulse is smallest for Mon 2 at around 3 mV. For both Mon 1 and Mon 3 the variation is around a factor two larger, at 6 mV.

#### 1.7.4 Zero Crossing

The full fit to the calibration result that is performed is:

$$\text{Mixer} = A \sin(bx + c) + d \quad (1.37)$$

Where  $x$  is the phase shifter setting.  $A$  and  $d$  are the calibration constants used to reconstruct the phase, with their values already quoted in Table ???. The remaining fit parameters  $b$  and  $c$  convert the phase shifter setting in to the phase offset between the LO and the beam. As the shifter readings are approximately in 4 GHz degrees, the expected value for  $b$  that converts the shifter value in to 12 GHz radians is  $(12/4) * (\pi/180) \simeq 50$  mrad/unit.

To obtain the best resolution for the measurement the mixers should be operated where the dependence of the output voltage on the phase is maximal. This means maximising the partial derivative of the mixer output with respect to the phase shifter setting:

$$\frac{\partial \text{Mixer}}{\partial x} = Ab \cos(bx + c) \quad (1.38)$$

This is maximised when  $bx + c = n\pi$ , where  $n$  is any positive or negative integer. The optimal phase shifter settings therefore meet this criteria:

$$x = \frac{n\pi - c}{b} \quad (1.39)$$

Where the mixer output is  $\text{Mixer} = A \sin(n\pi) + d = d$ . In the case where there is no offset between the minimum and maximum mixer output ( $d = 0$ ) the optimal point to operate the mixers is at zero output. Because of this the optimal shifter setting will be referred to as the zero crossing. In reality the small asymmetry in the mixer output means the optimal shifter setting is where mixer output is  $d$ . The effect of operating the mixers away from the zero crossing on the resolution is shown in Section ??.

In addition, as previously mentioned the convention is to operate the mixers on the falling slope where the partial derivative above is negative. The set shifter values are obtained using

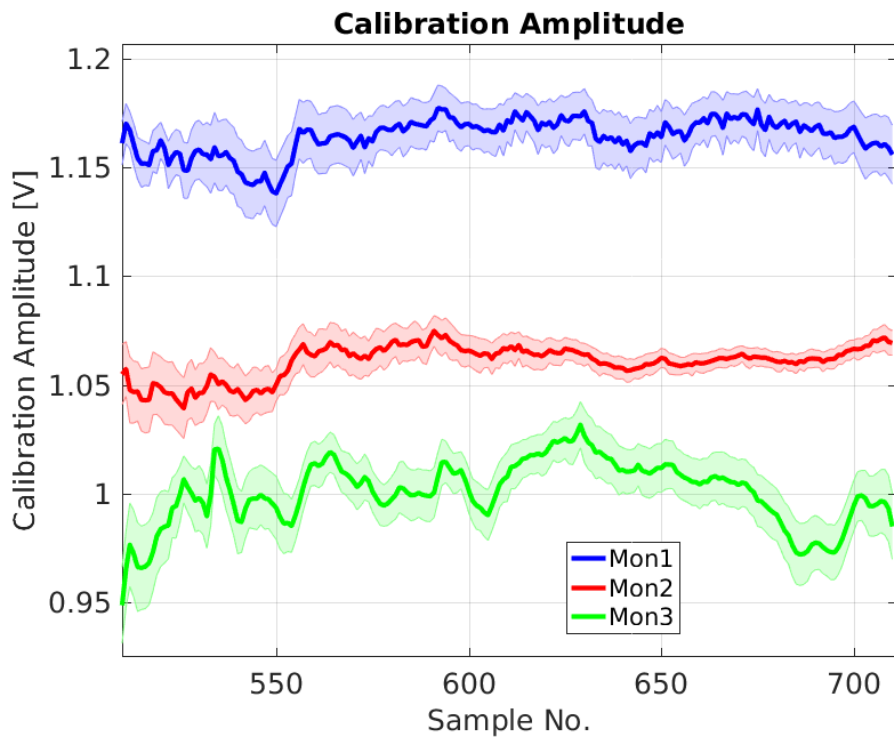


Figure 1.34: Variation in fitted amplitude along the pulse for each phase monitor.

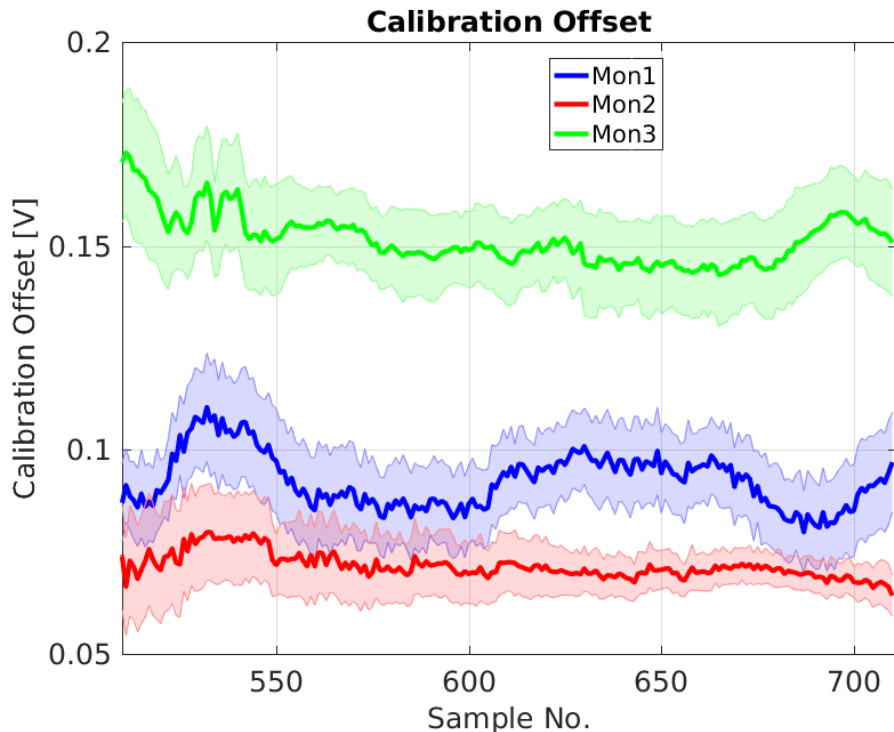


Figure 1.35: Variation in fitted offset along the pulse for each phase monitor

Monitor	$b$	$c$	Zero Crossing
Mon 1	$50.8 \pm 0.5$ mrad/unit	$2.29 \pm 0.04$ rad	$16.7 \pm 0.9$ units
Mon 2	$47.4 \pm 0.5$ mrad/unit	$1.36 \pm 0.04$ rad	$37.5 \pm 0.8$ units
Mon 3	$51.3 \pm 0.6$ mrad/unit	$4.02 \pm 0.04$ rad	$105.5 \pm 1.5$ units

Table 1.9: Phase shifter setting to obtain the zero crossing for each mixer output and the fit parameters needed to calculate them.

the smallest positive integer  $n$  that leads to this criteria being met. Table 1.9 shows an example of values for the fit parameters  $b$  and  $c$  and the calculated phase shifter settings to be on the zero crossing for each monitor. These values are taken from the same calibration and sample number presented in Section 1.7.1 (on the SiS digitisers). The reader may be interested to compare where the shifter settings fall along the mixer output traces during the calibration in Figure ??.

Due to the large phase sag along the beam pulse it is clearly not possible to be at the zero crossing of the mixer for the full pulse length. For the PFF system the region of interest is the central portion of the pulse where the phase sag is flattest. The shifters are therefore set to zero the mixer output in this region, giving best resolution in the central part of the pulse but degraded resolution near the start and end of the pulse. In addition to this, slow drifts in the beam phase, particularly downstream, mean that the shifters must routinely be changed to stay at the zero crossing. With the current setup using mechanical phase shifters this must be done by hand, with no possibility to implement an automatic feedback on the shifter settings, for example.

## 1.8 Phase Shifter Noise

In the first tests with all three phase monitors in their final positions at CTF3 the measured phase resolution was far in excess of the  $0.14^\circ$  derived to be necessary to achieve a  $0.2^\circ$  corrected downstream phase jitter in Section 1.3. Figure 1.36 shows a typical example of the measured resolution along the pulse at that time with an achieved resolution of around  $0.4^\circ$ , three times larger than required. The lowest downstream phase jitter that could be achieved with the PFF system in these conditions is above  $0.55^\circ$ , only about 30% smaller than the initial upstream phase jitter at CTF3 (Chapter ??). To be able to achieve a large reduction in downstream phase jitter with the PFF prototype the source of the poor phase monitor resolution had to be identified and removed.

The first hint towards identifying the cause of the degraded resolution came by comparing the measured phase jitter from Mon 1 and Mon 2, with one example shown in Figure 1.37. Note that for all the results in this section it is not the absolute value of the phase jitter (which depends mostly on the beam conditions in that dataset) that is important but rather the difference between the measured phase jitter in each monitor. The measured phase jitter along the pulse in Mon 2 with a mean of  $1.38 \pm 0.01^\circ$  is 1.7 times larger than the  $0.83 \pm 0.01^\circ$  phase jitter in Mon 1. Jitter values from this and all the other datasets presented in this

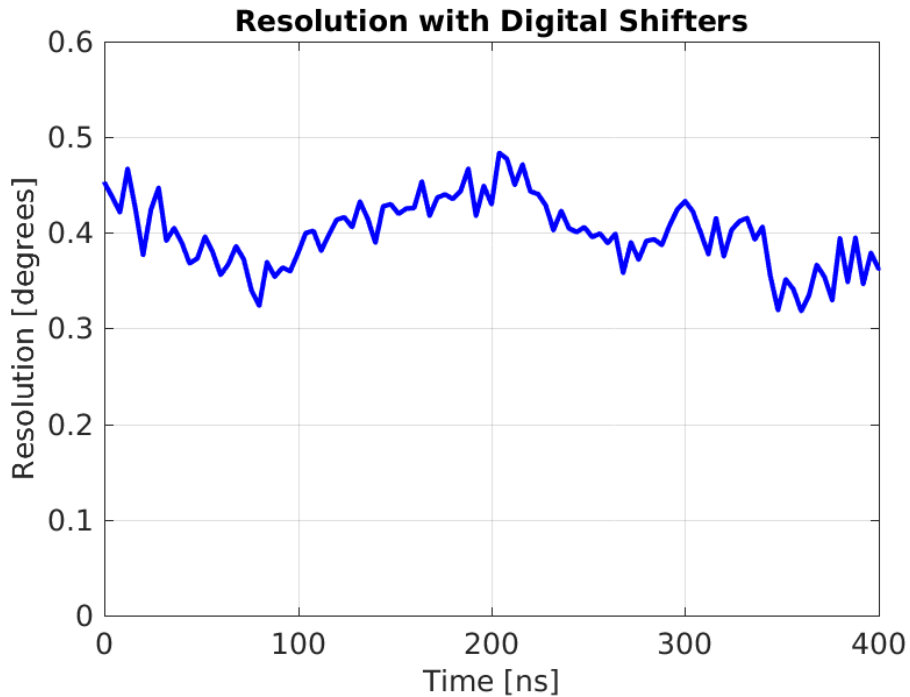


Figure 1.36: Phase monitor resolution using initial setup with digital phase shifters in place.

section are shown in Table 1.10. As Mon 1 and Mon 2 are neighbouring each other in the beam line the actual phase jitter in the two should be close to identical.

The overall phase monitor and electronics setup can be roughly split in to three systems – the RF signal from the beam (dependent on the phase monitors themselves and the hybrids), the LO reference signal and the mixers. An issue with any one of these systems could explain the larger phase jitter measured from Mon 2 (usually connected to Mixer 2 and LO 2) compared to the phase jitter from Mon 1 (usually connected to Mixer 1 and LO 1). To determine whether the issue was with the RF signal of one of the monitors measurements were taken with Mon 1 and Mon 2 swapped between the three mixers.

Figure 1.38 shows the measured phase jitter along the pulse when Mon 2 is moved on to Mixer 1 (and LO 1) and with Mon 1 moved on to Mixer 2 (and LO 2). The colours in all the plots in this section correspond to the mixer that measurement is from – blue for Mixer 1, red for Mixer 2 and green for Mixer 3. With the phase monitors swapped the higher measured phase jitter stays with Mixer 2 with the same ratio of 1.7, in this case  $1.48 \pm 0.01^\circ$  on Mixer 2 (connected to Mon 1) and  $0.89 \pm 0.01^\circ$  on Mixer 1 (connected to Mon 2). This rules out that the difference in phase jitter is coming from the phase monitors themselves, and suggests the problem is with either Mixer 2 or the reference signal LO 2 for that mixer. The same exercise can then be repeated with Mon 2 moved on to Mixer 3 (and LO 3) and the nominal setup used for Mon 1. Mixer 3 gives similar results to Mixer 2, with 1.7 times larger phase jitter than Mixer 1. This is seen in Figure 1.39. The remaining task is therefore to identify whether the additional source of noise is from Mixer 2 or LO 2, and from Mixer 3 or LO 3.

This was determined by swapping the LO reference signals between the mixers. Fig-

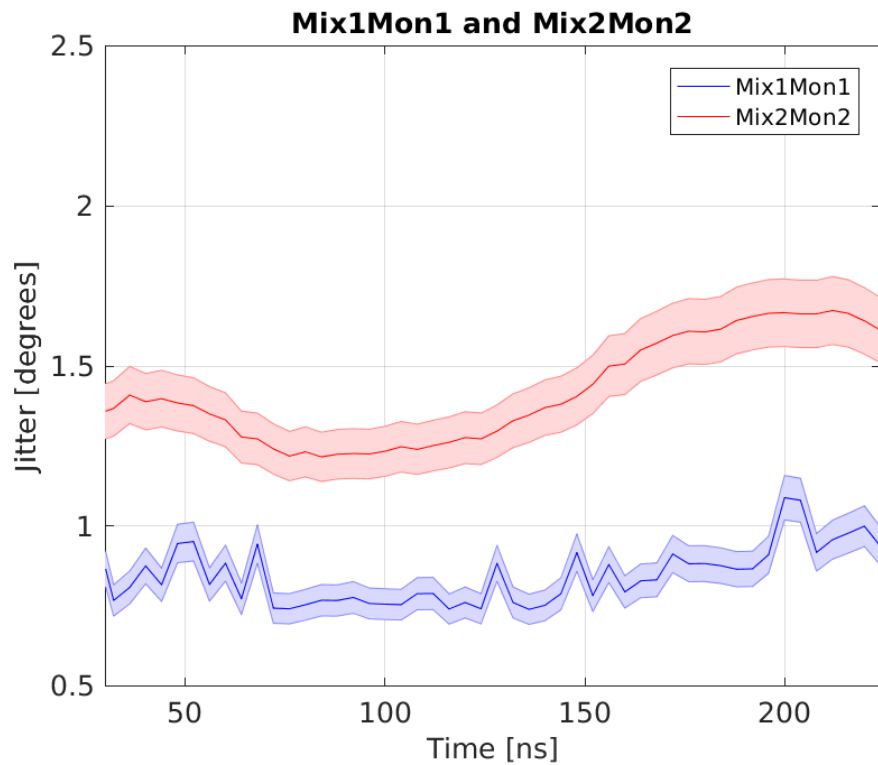


Figure 1.37: Phase jitter along the pulse with the nominal electronics setup – Mon 1 connected to the first mixer, and Mon 2 connected to the second mixer.

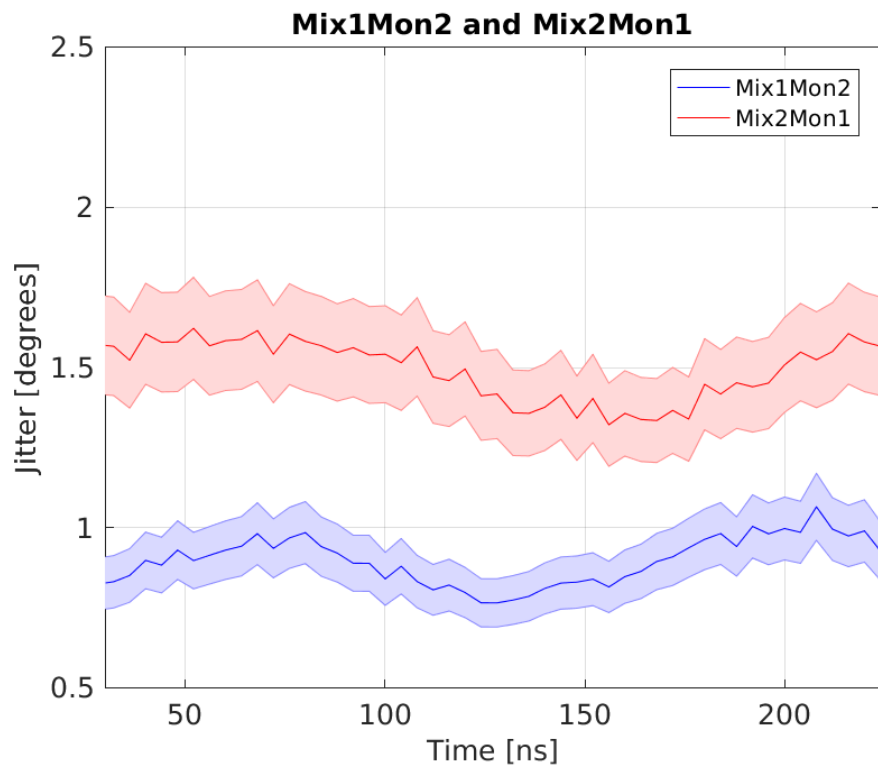


Figure 1.38: Phase jitter along pulse with Mon 2 connected to the first mixer and Mon 1 connected to the second mixer.

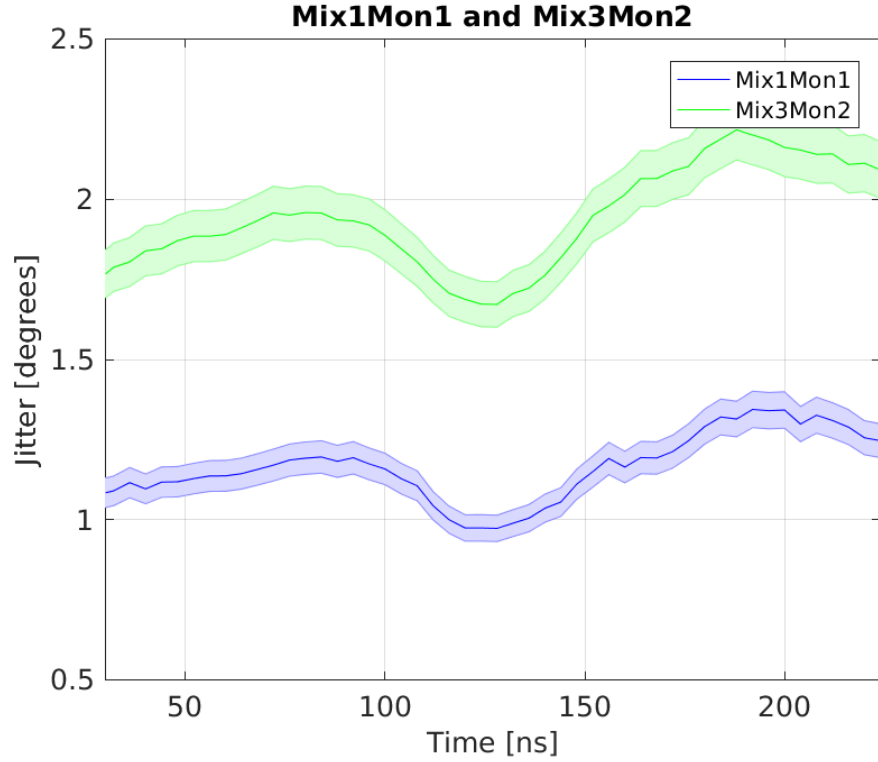


Figure 1.39: Phase jitter along pulse with Mon 1 connected to the first mixer and Mon 2 connected to the third mixer.

ure 1.40 shows the measured phase jitter with LO 2 connected to Mixer 1, and LO 1 connected to Mixer 2. In this case the lower measured phase jitter stays with LO 1, with  $1.10 \pm 0.01^\circ$  jitter on Mixer 2 (with LO 1) and  $1.68 \pm 0.01^\circ$  on Mixer 1 (with LO 2). In Figure 1.41 the same is seen with LO 3 connected to Mixer 1, and LO 1 connected to Mixer 3, with the lower phase jitter coming from Mixer 3 (LO 1) in this case. In Table 1.10 it can also be seen that the lowest phase jitter in every dataset always comes from the phase monitor for which LO 1 was used.

In this way an issue with LO 2 and LO 3 was identified. The generation of the LO reference signals (Section 1.2) consists of a 3 GHz source that is common to all three signals, plus separate phase shifters, frequency multipliers (to create the 12 GHz reference) and amplifiers for each LO signal. The digital phase shifters were thought to be the most likely culprit to be adding noise in to the system, and preliminary tests replacing one of the digital phase shifters with a mechanical alternative provided an immediate gain in resolution. Finally, all three digital shifters were replaced with mechanical phase shifters (the specifications of the shifters were introduced in Section 1.2). With this setup the measured phase jitter for Mon 1 and Mon 2 is the same irrespective of which mixer or LO the signal is connected to, as shown in Figure 1.42. The final achieved resolution is presented in the next section.

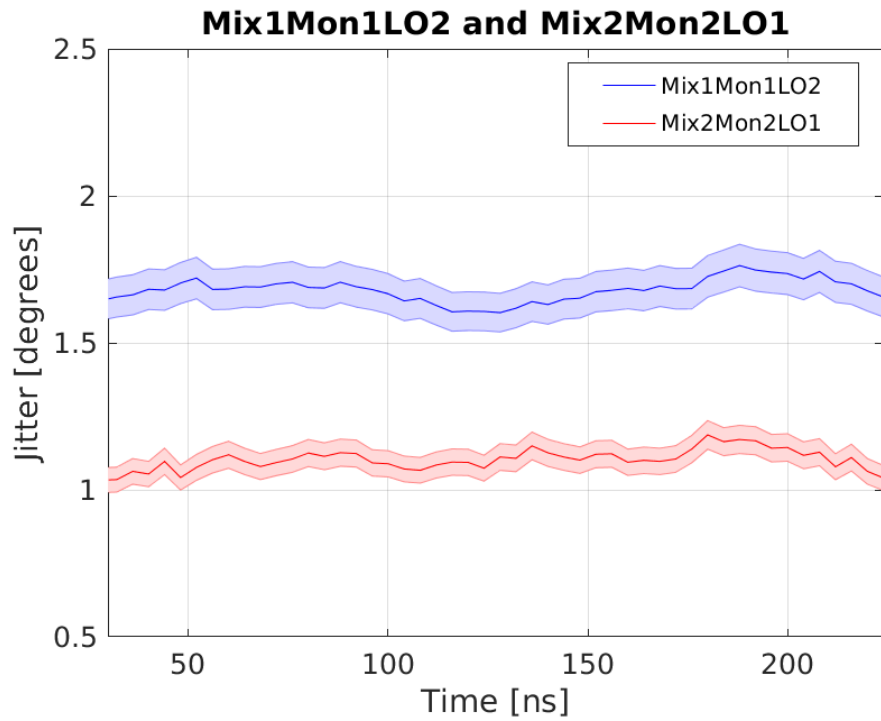


Figure 1.40: Phase jitter along pulse with the LO swapped between the first mixer and the second mixer.

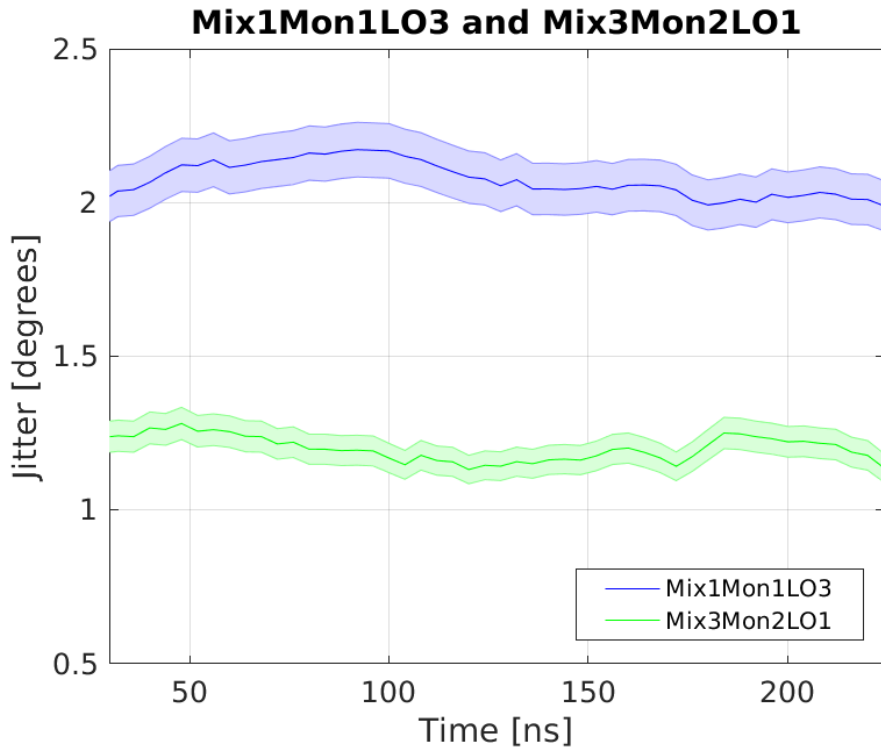


Figure 1.41: Phase jitter along pulse with the LO swapped between the third mixer and the first mixer.

Mon 1			Mon 2		
Mixer	LO	Jitter	Mixer	LO	Jitter
1	<b>1</b>	<b><math>0.83 \pm 0.01^\circ</math></b>	2	2	$1.38 \pm 0.01^\circ$
2	2	$1.48 \pm 0.02^\circ$	1	<b>1</b>	<b><math>0.89 \pm 0.01^\circ</math></b>
1	<b>1</b>	<b><math>1.15 \pm 0.01^\circ</math></b>	3	3	$1.91 \pm 0.01^\circ$
1	2	$1.68 \pm 0.01^\circ$	2	<b>1</b>	<b><math>1.10 \pm 0.01^\circ</math></b>
1	3	$2.07 \pm 0.01^\circ$	3	<b>1</b>	<b><math>1.20 \pm 0.01^\circ</math></b>

Table 1.10: Comparison of phase jitter along the pulse for each measurement with different setups of the electronics. Each row corresponds to the results of one dataset. The left hand side of the table shows the results from Mon 1 in that dataset, and the right hand side of the table the results from Mon 2. Bold text indicates the lower jitter value in that dataset, all of which use LO 1.

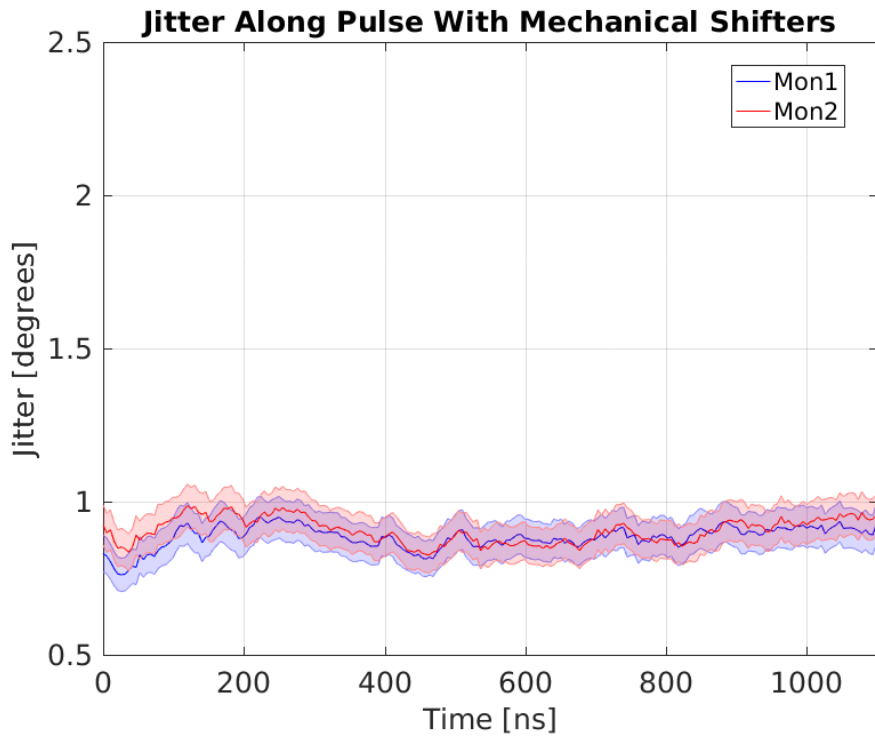


Figure 1.42: Phase jitter along pulse after installation of the mechanical phase shifters.

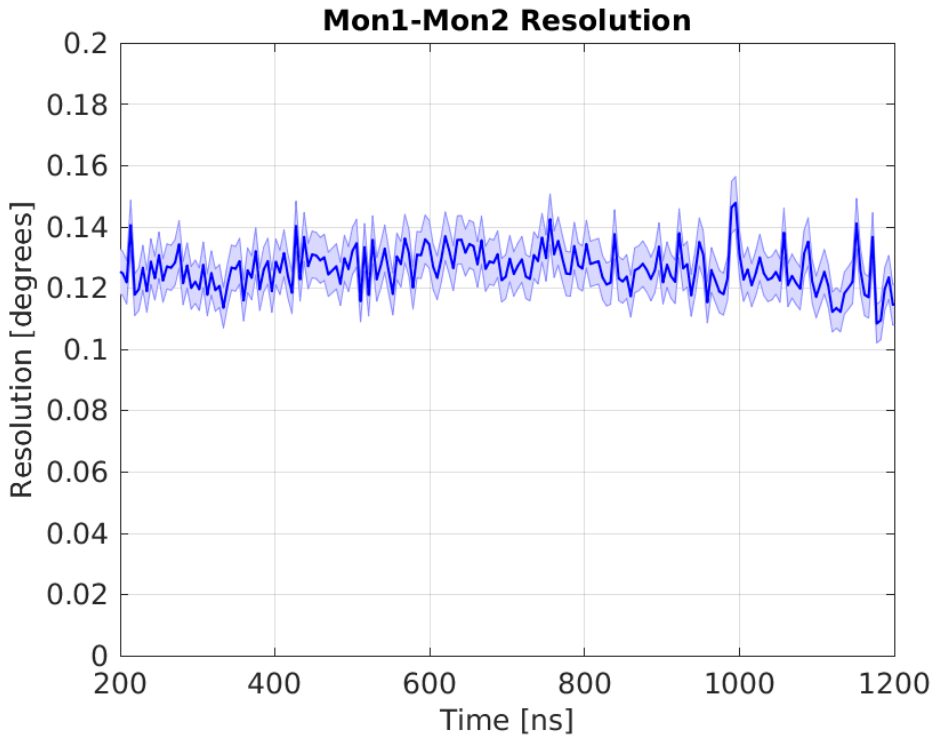


Figure 1.43: bestResolution

## 1.9 Resolution Measurements

This section presents resolution measurements with the mechanical phase shifters in place and the same overall electronics setup that was used to achieve the best PFF results in Chapter ???. All measurements use the upstream phase monitors Mon 1 and Mon 2. There is no way to directly verify the resolution of the downstream phase monitor Mon 3, but it should match that of Mon 1 and Mon 2 and the achieved phase stabilisation in Chapter ?? suggests it does have below  $0.2^\circ$  resolution.

### 1.9.1 Best Resolution

Figure 1.43 shows the best phase resolution that has been achieved to date sample by sample along the pulse. Each point corresponds to the phase jitter in the difference between the measured Mon 1 and Mon 2 phase divided by  $\sqrt{2}$  as per Equation 1.27. The resolution is quite stable along the pulse, with a mean value of  $0.1257 \pm 0.0005^\circ$ . This is below the  $0.14^\circ$  needed to be able to theoretically achieve a  $0.2^\circ$  correction with the PFF prototype, as derived in Section 1.3. The achieved resolution corresponds to a theoretical limit of around  $0.18^\circ$  in the corrected downstream phase jitter.

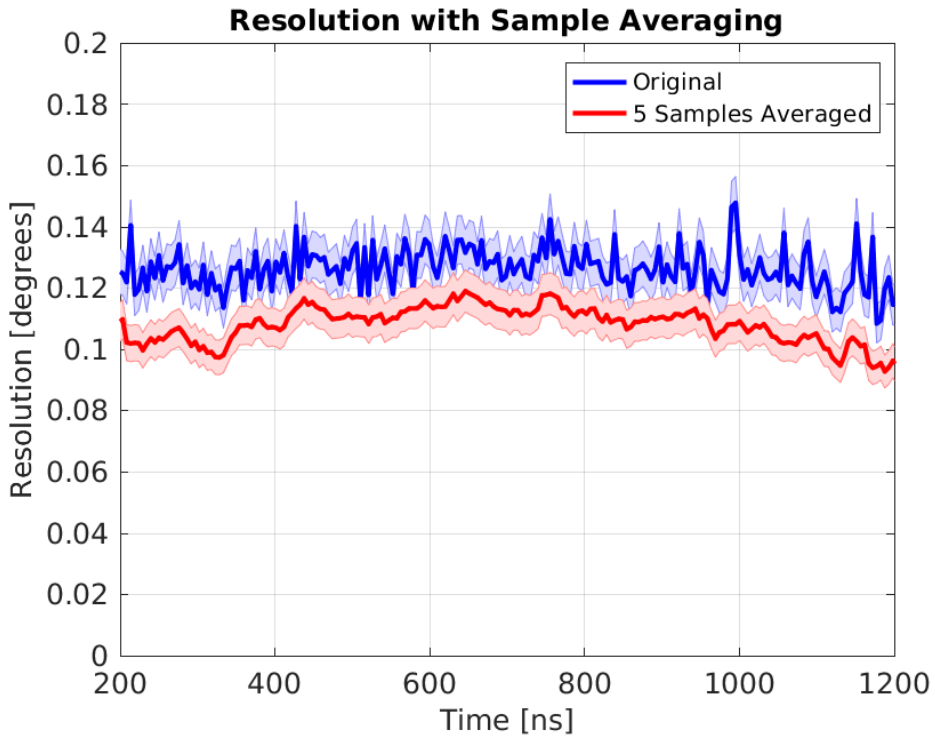


Figure 1.44: Effect on resolution by averaging samples.

### 1.9.2 With Sample Averaging

The phase monitor signals are digitised with a much higher sampling rate, 357 MHz on the FONT5a board or 192 MHz on the SiS digitisers, than the PFF correction bandwidth of around 30 MHz. This means the results from several samples could be averaged to reduce noise on the measurement whilst maintaining the same correction bandwidth. For example, for a measurement on the SiS digitisers, such as those shown here, 5 samples can be averaged to effectively create a signal with 38.4 MHz sampling rate, reduced from the initial 192 MHz. The effect of doing this is shown in Figure 1.44. The resolution is decreased from  $0.1257 \pm 0.005^\circ$  as seen previously to  $0.1077 \pm 0.0005^\circ$  with 5 samples averaged. Currently the phase propagation (Chapter ??) is the main limiting factor for the PFF performance rather than the phase monitor resolution. However, it would be possible to implement sample averaging in the PFF firmware on the FONT5a board if deemed necessary for future tests [REF].

### 1.9.3 Dependence of Resolution on LO Phase

The process of setting the mixers on their zero crossing after calibrations was documented in Section 1.7.4. This is necessary to operate the mixers where there output voltage is most sensitive to variations in the phase (close to the peaks of the mixer output there is negligible change in output voltage for small changes in phase). The dependence of the phase resolution on the beam phase across the full  $\pm 180^\circ$  range is shown in Figure 1.45. The plotted phase is the offset between the LO phase shifter setting and the calculated optimal setting. More

than  $50^\circ$  away from the zero crossing there is a large degradation in resolution, reaching above 1 degree at the  $+90^\circ$  peak.

However, for the PFF system the phase resolution only needs to be guaranteed within its correction range, which is close to  $\pm 6^\circ$  as seen in Section ???. In Figure 1.46 it is seen that there is no noticeable degradation in resolution in the range between  $\pm 15^\circ$ .

## 1.10 Bandwidth

The overall targeted bandwidth for the prototype PFF correction is **30 MHz**, which means each individual hardware component must have a bandwidth in excess of 30 MHz. To estimate the bandwidth of the phase measurement the delay loop has been used to create a sharp jump in the phase mid-way along the pulse. Normally the delay loop (whose length is 140 ns) is used with 1.5 GHz beam at CTF3, with seven 180 degree phase switches in the bunching at 140 ns intervals. Alternating 140 ns sub-trains are deflected in to the delay loop with a 1.5 GHz RF deflector, and then recombine with the 140 ns sub-trains bypassing the delay loop to double the drive beam current [REF]. If the delay loop is instead used with 3 GHz beam alternating bunches, rather than sub-trains, enter the delay loop. The first 140 ns of the pulse after the delay loop contains only bunches that bypassed the loop, so is a 1.5 GHz beam with half the initial beam current. After the first 140 ns there is a fast transition back to 3 GHz beam with the same initial current as delayed bunches merge with the bypassing bunches. By varying the length of the delay loop (using a wiggler [REF]) the phase of the bunches leaving the delay loop can be changed, also creating a fast phase jump at the transition to 3 GHz beam.

**Figure 1.47** shows the response of the Mon 3 mixer to a beam pulse with a phase step setup in this way. The first 140 ns of the pulse contains only bunches bypassing the delay loop, as described, followed by the fast transition to 3 GHz beam and the phase step. The time taken for the mixer output to respond to the fast phase change can be related to the bandwidth by this approximate relationship [REF]:

$$\text{BW} = \frac{350}{t} \quad (1.40)$$

Where BW is the bandwidth in MHz and  $t$  is the rise time of the signal in ns. The transition between the two phase states as seen on the mixer output occurs between 156.6 ns and 167.0 ns, a rise time of 10.4 ns corresponding to a bandwidth of approximately 34 MHz. In addition, the falling edge of the mixer output at the end of the pulse also takes around a 10 ns, also leading to a bandwidth estimate in the region of 35 MHz.

## 1.11 Comparison of Measured Phase Along Pulse

It has been shown that the phase jitter is at the **same level in each monitor** after the installation of mechanical phase shifters, and that the **achieved resolution is better than the level needed to be able to theoretically achieve a  $0.2^\circ$  PFF correction**. Nevertheless there are

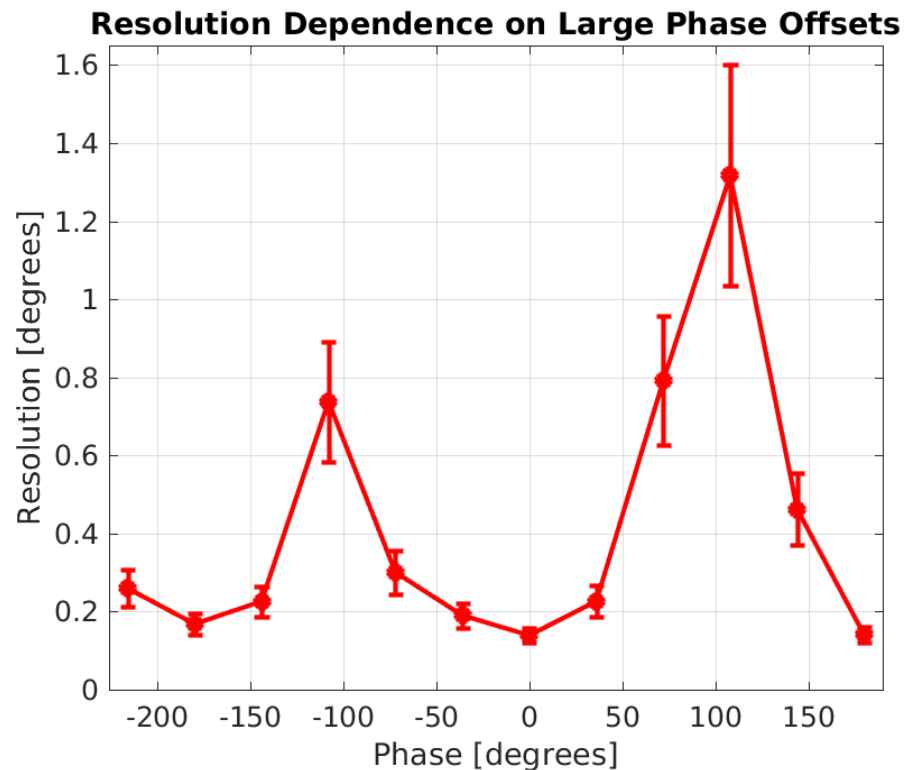


Figure 1.45: Resolution.

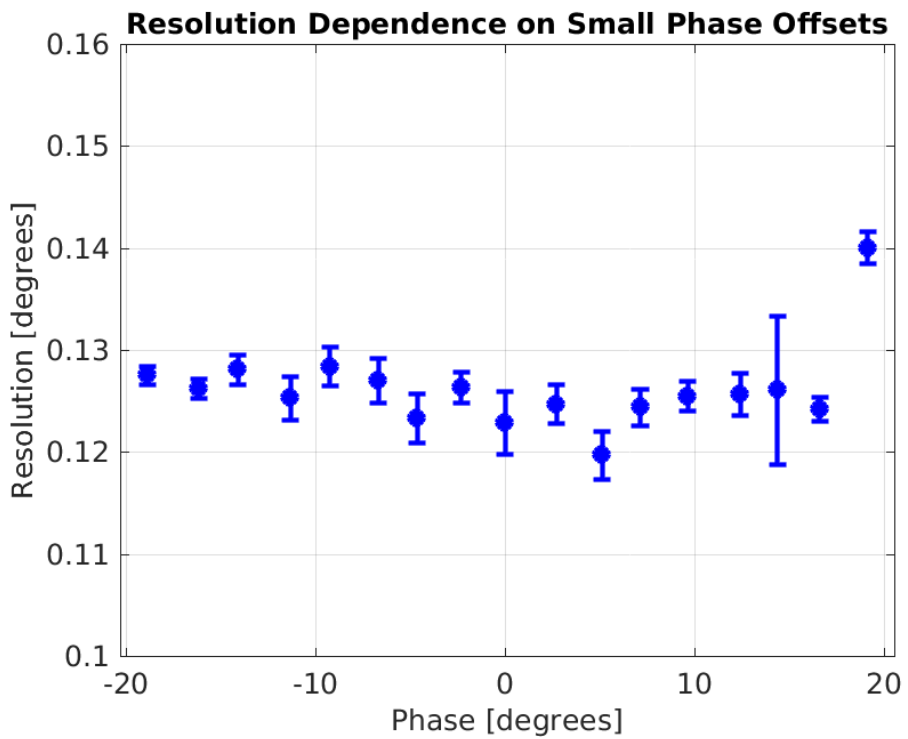


Figure 1.46: Resolution.

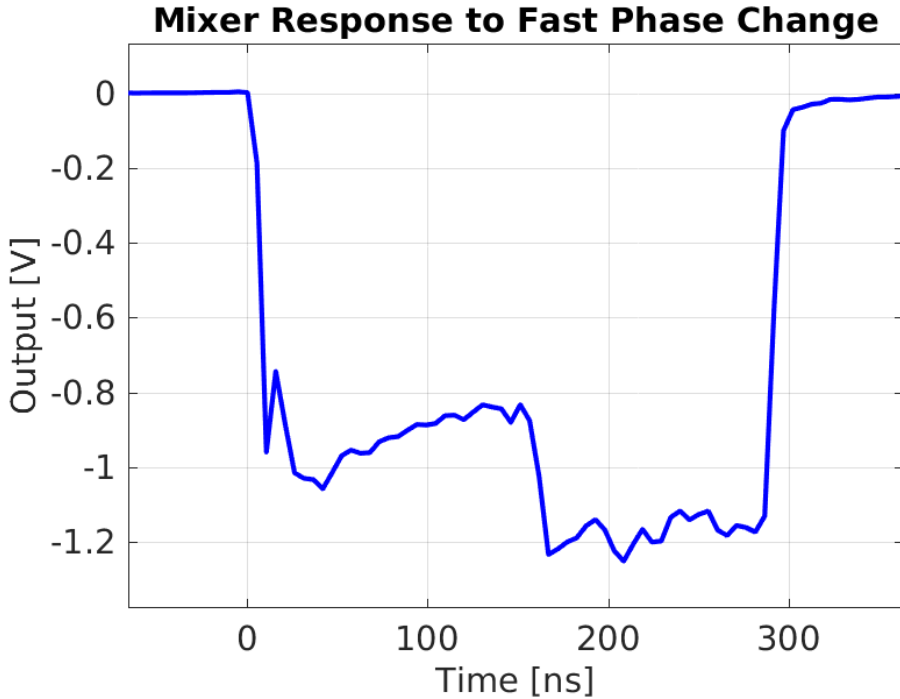


Figure 1.47: Response of Mixer 3 to a jump in phase in the middle of the pulse.

several remaining effects that have been identified which may limit the PFF performance in a way not described by the resolution. These are the focus of the remainder of this chapter, starting with differences between the measured shape of the phase along the pulse [here](#). Neither the phase jitter nor the resolution are sensitive to any static differences in the measured phase in each monitor. For the PFF system to remove not only phase jitter but also to flatten the phase sag along the pulse the shape of the upstream and downstream phase must be the same.

Figure 1.48 shows an example of the measured phase along the pulse in all three monitors, as well as a fourth phase measurement taken from one of the power extraction and transfer structures (PETS) in the TBL line after Mon 3 [REF]. The PETS measurement provides an independent cross-check of the response and calibration of the three PFF monitors. All four phase measurements show approximately the same overall phase sag of around 45° along the full pulse length, as desired.

Nevertheless, there are differences between the measurements. As described later in Chapter ?? there are many mechanisms by which the beam phase can change between the upstream and downstream monitors. Small discrepancies between the Mon 1 and Mon 2 phase compared to the Mon 3 and PETS phase are therefore not unexpected. However, as Mon 1 and Mon 2 are neighbouring each other in the beam line their measurements are expected to agree almost perfectly but this is not the case. At the start of the pulse the Mon 2 phase is around 6° lower than the Mon 1 phase, whereas at the end of the pulse the Mon 2 phase is around 2° higher than the Mon 1 phase, for example.

[Two possible explanations](#) could have been an error in the fitted calibration amplitude or a time offset between the two signals. The fact that the Mon 2 phase is lower at one end

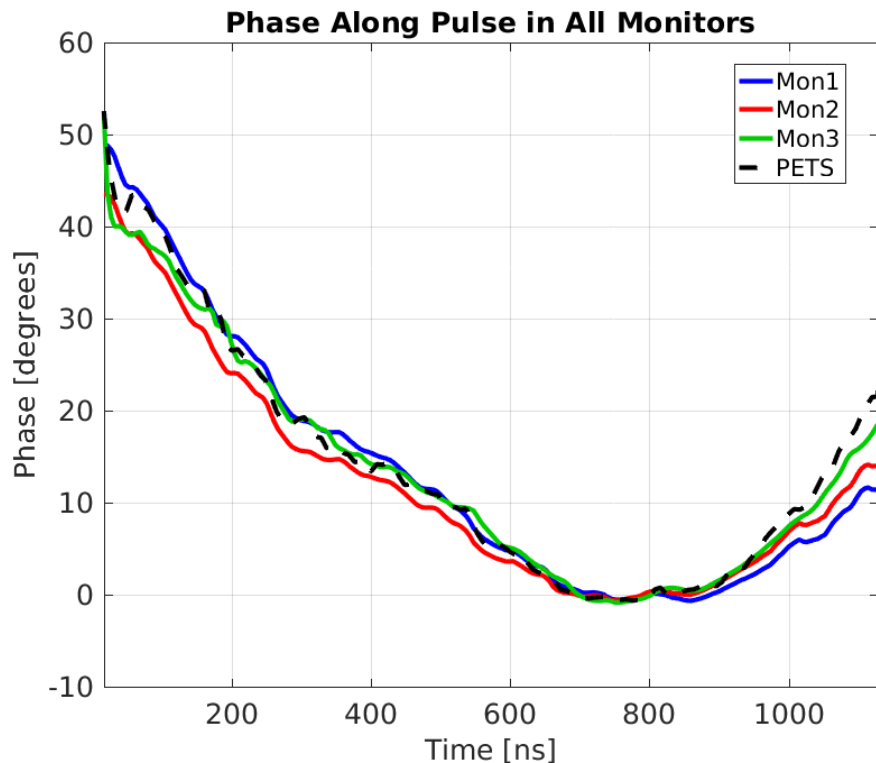


Figure 1.48: Comparison of phase along the pulse in the three PFF phase monitors and an alternative phase measurement from a PETS.

of the pulse but higher at the other means that the difference is not simply a scale factor between the two, and therefore cannot be described by an error in calibration amplitude. Neither can it be explained by differences in the calibration constants along the pulse, as seen in the next section. Similarly, by observing small variations along the pulse, for example at the end of the pulse after a time of 1000 ns in the figure, it can be seen that the two measurements are well aligned in time.

The blue line in Figure 1.50 shows the difference between the Mon 1 and Mon 2 phase along the pulse. The offset between the two has a clear linear dependence on the time along the pulse. As a result, one way in which the agreement between the two measurements can be improved is by rotating Mon 2 with respect to Mon 1 about a time of 850 ns where the offset between the two is zero. With an optimal rotation of  $2.1^\circ$  the mean absolute offset between Mon 1 and Mon 2 between 370 ns and 1080 ns can be reduced from  $1.44 \pm 0.08^\circ$  to  $0.12 \pm 0.01^\circ$ . The red line in the figure shows the difference along the pulse after performing this rotation. Figure 1.48 then shows a comparison between the mean phase along the pulse in Mon 1 and Mon 2 after the rotation, with the original measurement from Mon 2 also shown for reference. The agreement in shape between the two is now excellent, with only a slight discrepancy at the end of the pulse.

The source of this apparent rotation between Mon 1 and Mon 2 is not clear and could be an effect of the monitors themselves, the calibration process or a real difference between the beam phase in each monitor. If there was a real rotation in the phase sag between monitors or if there was an issue with Mon 1, used as the PFF correction input, it would

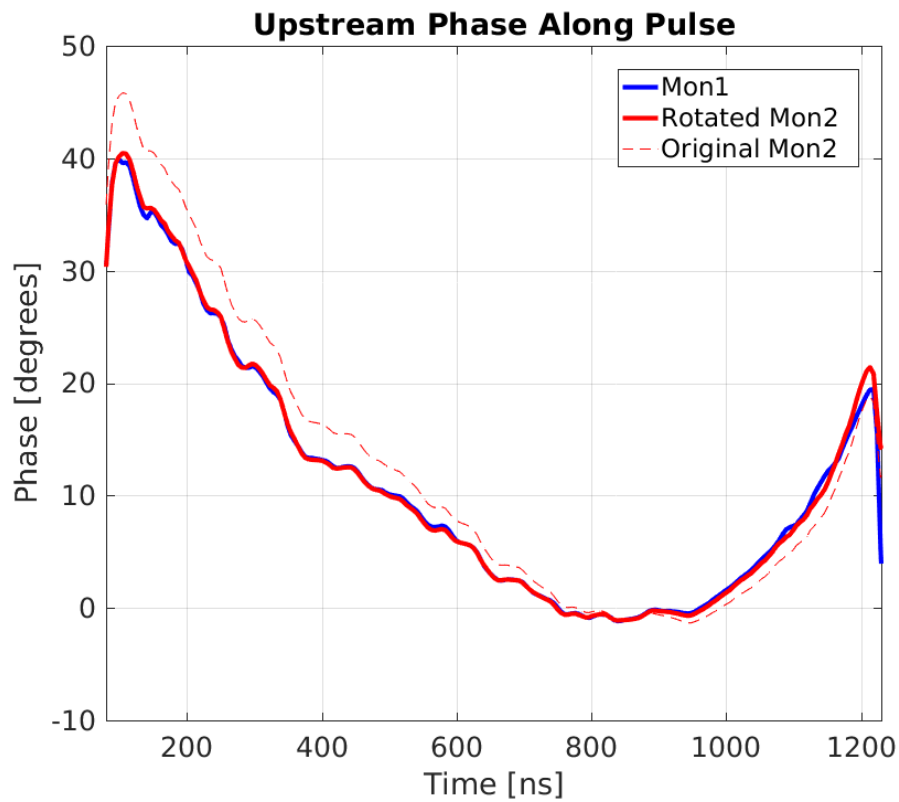


Figure 1.49: Comparison of Mon 1 and Mon 2 phase along the pulse, with Mon 2 rotated by  $2.1^\circ$  about a time of 850 ns on the horizontal axis.

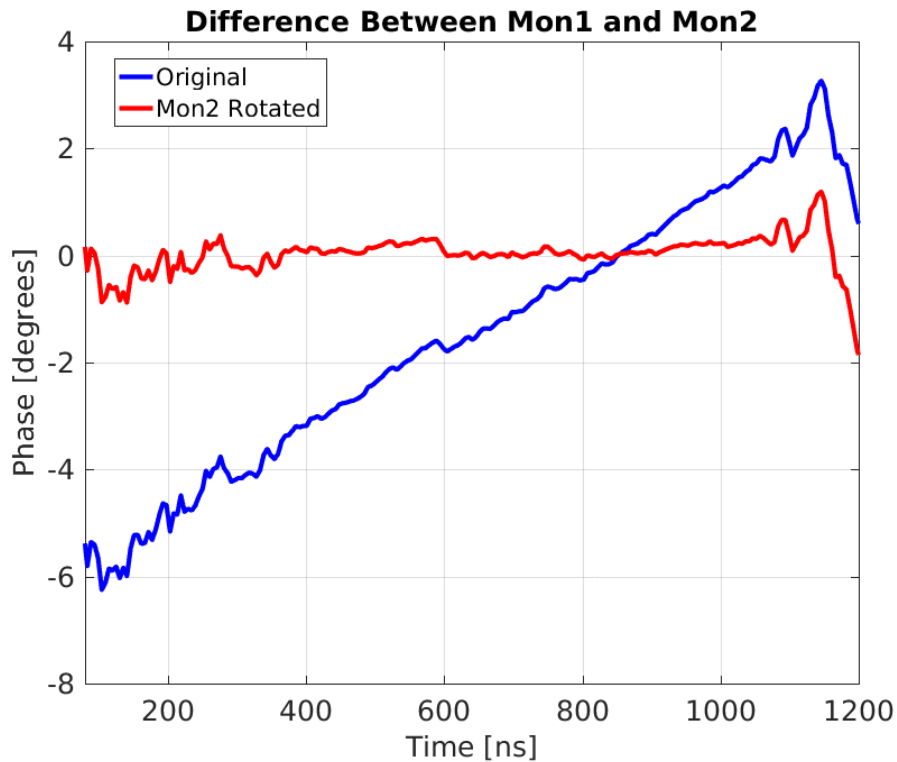


Figure 1.50: Difference between Mon 1 and Mon 2 phase along the pulse with and without Mon 2 rotated.

not be possible to completely flatten the phase sag along the pulse with the PFF system. The excellent flattening of the pulse that has in reality been achieved with the PFF system (Chapter ??) suggests this may be an issue affecting only Mon 2, as the correction input is based solely on Mon 1. An issue with the measured pulse shape from Mon 2 may also help to explain differences between the shape of the applied kick and the upstream phase (measured by Mon 2) seen later in Section ??.

## 1.12 Effect of Variations in Calibration Constant

In Section 1.7.3 it was shown how the calibration parameters vary along the pulse. In the PFF algorithm, and usually also in data analysis, single values for each calibration constant are used across the full pulse length. This will lead to small discrepancies between the measured phase and the true beam phase. Examples of the size of this effect are shown in Figures 1.51, for Mon 2, and in Figure 1.52 for Mon 3, comparing the measured phase along the pulse when using single value calibration constants or varying calibration constants along the pulse. In the range between 600 ns and 1000 ns around the middle of the pulse where the phase sag is flattest (the part of interest for the PFF system) using a varying calibration constant along the pulse makes almost no difference to the measured upstream phase. This is unsurprising as the calibration constants normally used are calculated from one sample in this range. Outside this range the difference between the two reaches a peak of  $1.5^\circ$  near the start of the pulse.

For the downstream phase the differences are larger, including up to  $1.5^\circ$  offsets between the two methods in the range of interest for the PFF system. However, the example shown is without fully optimised downstream beam conditions achieved in Chapter ?? and so represents a worst case scenario for normal PFF operation. The PFF correction quality also does not directly depend on the downstream phase measurement (apart from for the gain calculation, as derived in Section ??), so these differences can be removed in offline analysis if deemed necessary.

## 1.13 Dependence on Position

As discussed in Section 1.1 the phase monitor output from the two vertical RF feedthroughs are summed in hybrids, and it is this sum signal that is connected to the mixers. This reduces, but does not remove completely, the dependence of the phase monitor signal power on the beam position in the monitor. In this section the remaining position dependence of the phase measurement is determined. Understanding the magnitude of the effect is particularly important considering the diodes are no longer used to power normalise the mixer output as originally intended.

The magnetic corrector placed roughly 1 m prior to Mon 1 (labelled CT.DHD0360) has been used to scan the beam position in the upstream phase monitors both horizontally and vertically. Around 1 m following Mon 2 there is a quadrupole (CT.QFF0420) followed by a

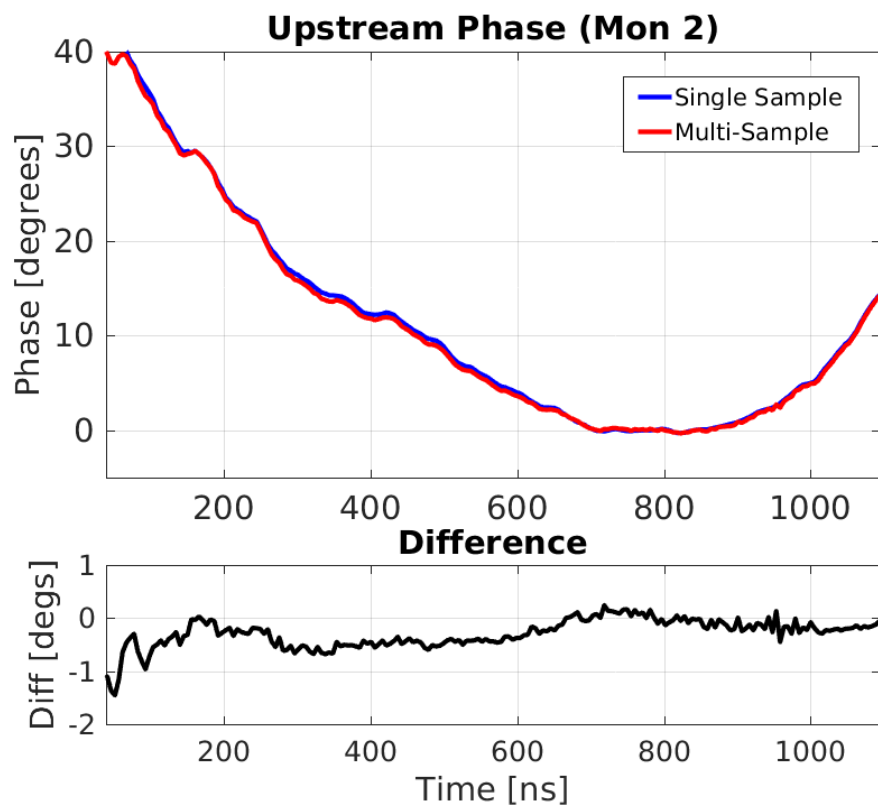


Figure 1.51: Effect of using a varying calibration constant on the upstream phase.

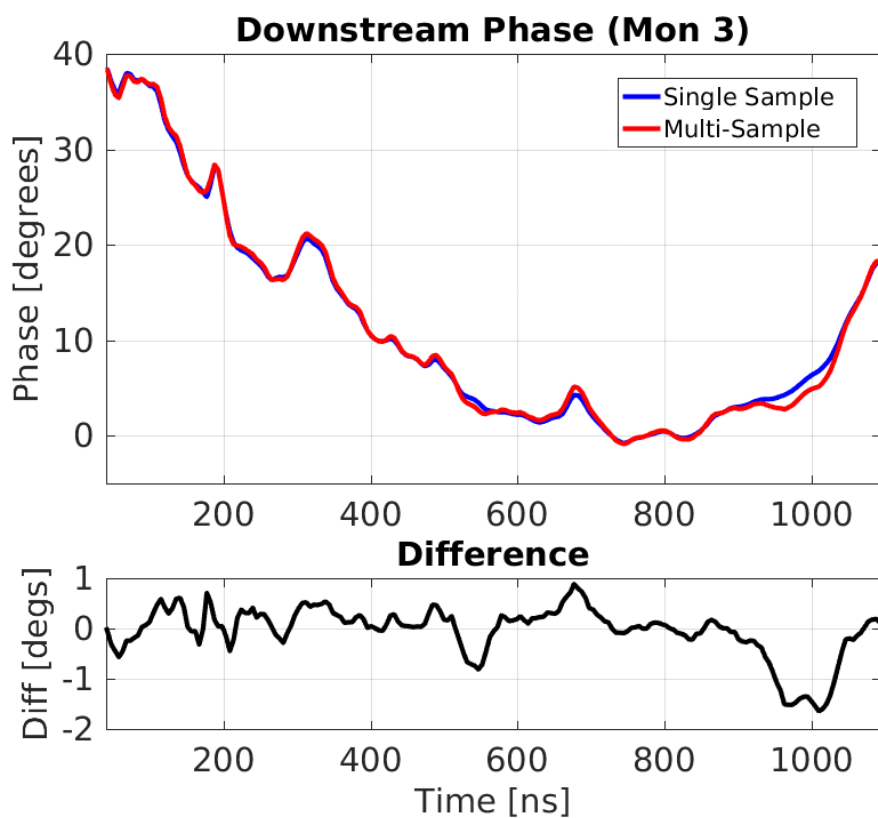


Figure 1.52: Effect of using a varying calibration constant on the downstream phase.

Device	Distance From CT.0360	Label
Mon 1	104.5 cm	$s_{M1}$
Mon 2	144.5 cm	$s_{M2}$
CT.BPM0430	357.0 cm	$s_{430}$

Table 1.11: Distance of the upstream phase monitors and following BPM CT.0430 to the corrector CT.0360 before the phase monitors.

beam position monitor or BPM (CT.BPM0430). For the purposes of this measurement the quadrupole is turned off so that the whole 3.5 m length of beam line between the corrector and the BPM is a drift space. It is then straightforward to reconstruct the position offset in the two phase monitors based on the BPM measurement without having to rely on the MADX model to take in to account the effect of the quadrupole on the beam orbit. The position of the corrector with respect to the phase monitors can be seen in Figure 1.4. Distances between the elements are shown in Table 1.11.

In these conditions a position offset of  $x_{430}$  measured in the BPM (in horizontal or vertical) corresponds to the following position offsets,  $x_{M1}$  and  $x_{M2}$ , in each phase monitor:

$$x_{M1} = r_{M1}x_{430} \quad (1.41)$$

$$x_{M2} = r_{M2}x_{430} \quad (1.42)$$

Where  $r_{M1}$  and  $r_{M2}$  are the position offsets in the phase monitors per unit position offset in the BPM, given by:

$$r_{M1} = \frac{s_{M1}}{s_{430}} \quad (1.43)$$

$$r_{M2} = \frac{s_{M2}}{s_{430}} \quad (1.44)$$

Where  $s_{M1}$ ,  $s_{M2}$  and  $s_{430}$  are the distances between the corrector and the phase monitors ( $s_{M1}$ ,  $s_{M2}$ ) or BPM ( $s_{430}$ ). Substituting in the values from Table 1.11 gives values of  $r_{M1} = 0.29$  and  $r_{M2} = 0.41$ .

Figure 1.53 shows the results of a horizontal position scan in the upstream phase monitors, with the phase plotted against the horizontal position in the BPM. Position scans of this type require a long time to complete in order to be able to acquire enough statistics at multiple corrector settings. The scan presented represents a data taking period of around one hour, for example. This means real drifts in beam phase (aside from any position dependent effects on the monitor signals) are unavoidable during the scan. The first impression of Figure 1.53 is that the only visible change in measured phase is due to actual drifts in beam phase rather than being as a result of the changes in position. However, Figure 1.54 shows the response of the phase monitor diode signals to the horizontal position in the BPM during the scan. Even though the diodes are heavily saturated a dependence of their output, and so a dependence of power, on the position is visible. This suggests there should also be a visible effect on the phase.

To remove the effects of drifts in the beam phase the difference between the measured Mon 1 and Mon 2 phase can be considered instead. The true beam phase,  $\phi_b$ , should be

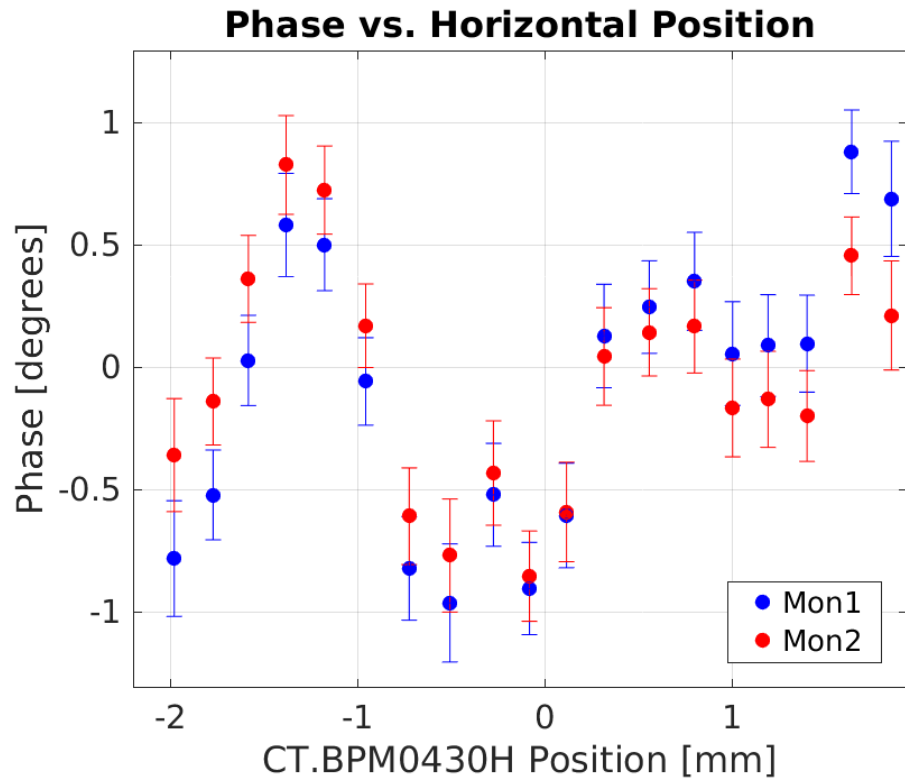


Figure 1.53: Mon 1 and Mon 2 phase dependence on horizontal position during scan.

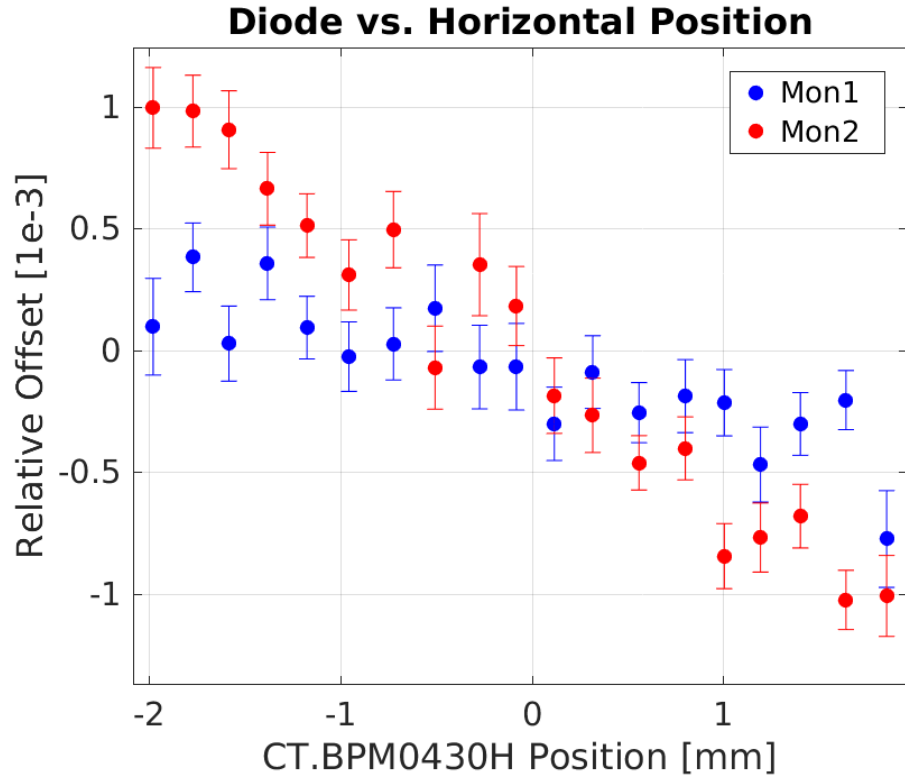


Figure 1.54: Mon 1 and Mon 2 diode dependence on horizontal position during scan.

identical in Mon 1 and Mon 2, so any differences between their measurements  $\phi_{M1}$  and  $\phi_{M2}$  during the scan can be modelled as coming from the beam position in the monitor, as follows:

$$\phi_{M1} = \phi_b + c_{M1}x_{M1} \quad (1.45)$$

$$\phi_{M2} = \phi_b + c_{M2}x_{M2} \quad (1.46)$$

Where  $c_{M1}$  and  $c_{M2}$  are constants expressing the phase shift per unit position offset in each monitor. The difference between the measured phase in Mon 1 and Mon 2 is therefore given by:

$$\phi_{M2} - \phi_{M1} = c_{M2}x_{M2} - c_{M1}x_{M1} \quad (1.47)$$

$c_{M1}$  and  $c_{M2}$  cannot be determined individually from the scan results alone using this approach, so instead it will be approximated that the strength of the position dependence is the same in Mon 1 and Mon 2. Letting  $c_{M1} = c_{M2} = c$  finally gives:

$$\phi_{M2} - \phi_{M1} = c(x_{M2} - x_{M1}) \quad (1.48)$$

$$c = \frac{\phi_{M2} - \phi_{M1}}{x_{M2} - x_{M1}} \quad (1.49)$$

The expressions for  $x_{M1}$  and  $x_{M2}$  in terms of the BPM position  $x_{430}$  derived earlier can then be substituted in to give:

$$c = \frac{\phi_{M2} - \phi_{M1}}{x_{430}(r_{M2} - r_{M1})} \quad (1.50)$$

The gradient of the phase difference versus the position offset in the BPM,  $(\phi_{M2} - \phi_{M1}) / x_{430}$ , is the only remaining parameter left to calculate in order to estimate  $c$ .

Figure 1.55 shows how the difference between the Mon 1 and Mon 2 phase measurement depends on the horizontal position in the BPM during the scan. By removing the actual beam phase drifts the dependence of the phase measurements on the beam position becomes clear. The fitted gradient is  $-0.22 \pm 0.01^\circ$  per mm offset in the BPM. Using Equation 1.50 this corresponds to a phase shift of  $-1.84 \pm 0.07^\circ$  per mm offset in the phase monitors themselves.

Exactly the same process can be repeated in the vertical plane, and the results of doing this are shown in Figure 1.56. Although the effect is smaller there is still a visible dependence of the phase on the vertical position, in this case with a gradient of  $0.06 \pm 0.01^\circ$  per mm offset in the BPM corresponding to  $0.53 \pm 0.07^\circ$  per mm vertical offset in the phase monitors.

The position dependence of the measurement appears large when quoted like this but it must be remembered that millimetre scale changes in beam orbit are rare during normal operation. Orbit jitter at CTF3 around the location of the upstream phase monitors is typically at the 0.02 mm level [REF]. Taking the calculated position dependence of Mon 1 and Mon 2 this corresponds to only an additional measured phase jitter of roughly  $0.04^\circ$ , using the larger dependence in the horizontal plane. This is only a small contribution to the overall phase monitor resolution of around  $0.13^\circ$  as seen in Section 1.9. However, it is important to consider that any change in beam setup that alters the trajectory through the monitors will lead to a change in output power and therefore a change in calibration constants. Calibrations are always repeated when the CTF3 setup is changed to take this in

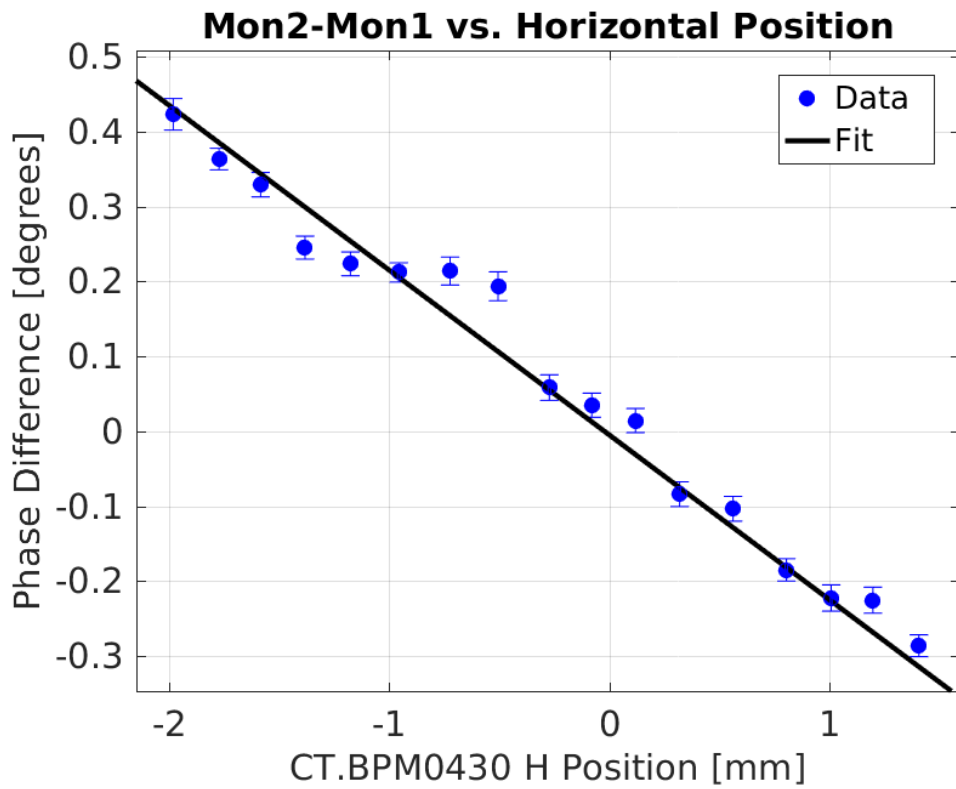


Figure 1.55: Fit to difference between Mon 1 and Mon 2 phase versus horizontal position.

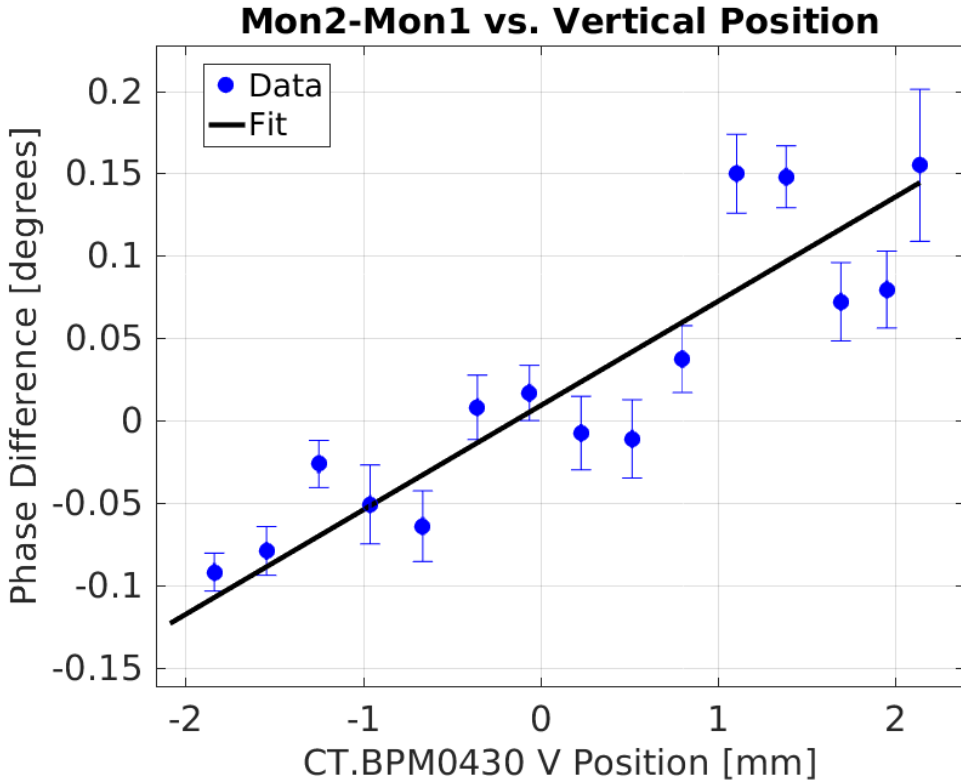


Figure 1.56: Mon 1 and Mon 2 dependence on horizontal position during scan.

to account. Position scans around the region of the downstream phase monitor Mon 3 would be much more difficult to perform and have not yet been attempted. The effect should be of a similar magnitude, although the downstream beam is less stable than upstream so the contribution to measured phase jitter is likely to be slightly larger.



# Bibliography

- [1] Dummy One & Dummy Two. *Phys. Journal*, **1**, 1 (2002) 1–5. hep-ph/0000000.  
<http://some.web.address>